patients (age range, 62–87 years old [y.o.]; mean, 73.7 y.o.) and 16 patients who died of nonneurological diseases (47–94 y.o.; mean, 64.1 y.o.). The frontal cortex and striatal tissues for immunoblot were dissected at Kyoto University Hospital and Juntendo Hospital, respectively, quickly frozen, and preserved at −80°C until protein extraction (see Supplemental Figure S1 for clinical data). In each case, the clinical diagnosis was confirmed neuropathologically, mostly by the presence of nigral LBs by hematoxylin-eosin stain. For immunohistochemistry, the brains fixed with 4% paraformaldehyde were sliced coronally, and the cerebral region containing the basal ganglia was isolated and embedded in paraffin, sectioned (6 μm thick), and subjected to immunohistochemistry as previously described (Ihara et al., 2003). The immunostained sections were optically scanned (16 bit, 600 dpi), and the integrated densities for a selected area (2 mm × 2 mm) were calculated with software (MultiGauge 2.0, Fujifilm, Japan). In each sample, three or more areas of the putamen and insular cortex were measured to obtain the average densitometric values.

Double-Label Immunofluorescence

Double-labeling immunofluorescence studies were performed by incubating human and mouse tissue sections with anti-Sept4, -DAT, or -α-synuclein antibodies. Fluorescein isothiocyanate- or rhodamine-conjugated appropriate secondary antibodies were applied. See the Supplemental Data for details.

Comparative Morphometric Analyses of DA Nerve Terminals at Light Microscopy and EM Levels

High-contrast images of TH-stained mouse striatal sections were captured and digitized by a light microscope with a CCD camera. The digital images were binarized with an arbitrary threshold, and the total length of the TH-positive neurites was calculated using Neurocyte Image Analyzer, ver. 1.5 (Kurabo, Japan). For the EM-level measurement of DA nerve terminal area, we used immuno-EM images of TH and DAT. TH- or DAT-positive areas in each digital EM image displayed on a computer screen were encircled manually using a digital pen tablet system, Intuos3 (Wacom Technology, Japan). The total encircled area was automatically calculated with graphic software (Scion, ver. β 4.0.2.). For each marker, 24 fields from corresponding regions of dorsal striata of *Sept4*$^{+/+}$ and *Sept4*$^{-/-}$ littermates were randomly sampled and analyzed blindly.

Immunoblotting and Immunoprecipitation

For immunoblotting, striatal tissues punched out from coronal brain slices of 3–5 m.o. mice were homogenized and sonicated in buffer A (10 mM Tris-HCl [pH 7.6], 1% Triton X-100, 0.15 M NaCl, 0.1% sodium deoxycholate, 0.1% sodium dodecyl sulfate), and then centrifuged at 15,000 × g at 4°C for 0.5 hr. The protein content of the supernatants was quantified using the Bradford method, and 50 μg of protein was denatured with an equal volume of 2 × SDS sample buffer and subjected to a standard immunoblot assay using peroxidase-conjugated secondary antibodies and an ECL chemiluminescence kit (GE Healthcare Biosciences). The amount of immunoreactive proteins was estimated by densitometry (see above). For coimmunoprecipitation of proteins, tissues were extracted with buffer B (0.1 M Tris-HCl [pH 7.6], 1% Triton X-100, 0.1% sodium deoxycholate, 0.1% SDS, protease inhibitors). After centrifugation, the supernatants were diluted with nine volumes of lysis buffer B′ without Triton X-100, resulting in a final concentration of 0.1%. Each lysate was incubated with various antibodies and Affi-Prep Protein A beads (Bio-Rad) at 4°C for 1 hr. Immunoprecipitates on the beads were washed five times with lysis buffer A, and analyzed by immunoblot.

Animals and Experimental Design

All animal procedures were performed in accordance with the guidelines of the Animal Use and Care Committee of Kyoto University. Heterozygous *Sept4*$^{+/-}$ mice were backcrossed with C57BL/6J for at least ten generations (Ihara et al., 2005). *Sept4*$^{-/-}$ mice and the control littermates were generated from *Sept4*$^{+/-}$ mice. The original αS^{tg} mice were bred with *Sept4*$^{-/-}$ mice to generate $\alpha S^{tg}/S4^{+/-}$ mice, which were inbred to generate $\alpha S^{tg}/S4^{+/+}$, $\alpha S^{tg}/S4^{+/-}$, and $\alpha S^{tg}/S4^{-/-}$ littermates. Biallelic Tg mice were identified by real-time PCR analysis and verified by backcrossing. All comparisons were made between littermates to minimize confounding effects by different genetic backgrounds. All behavioral tests were carried out on male mice (2–2.5 m.o.) (Miyakawa et al., 2001). Mice were given a light/dark cycle of 12 hr (lights on at 7 a.m.) and food and water ad libitum. Behavioral testing was performed between 9 a.m. and 6 p.m. except for the home cage social interaction test. After each test, all apparatuses were cleaned with acidic hypochlorous solution that eliminated mouse odors. Mouse brains were dissected after deep anesthesia with sodium pentobarbital (50 mg/kg, i.p.) with or without transcardial perfusion with 0.01 M phosphate-buffered saline (PBS). For histological analysis, mice were additionally perfused with 4% paraformaldehyde and 0.2% picric acid in 0.1 M PBS. Tissues from symptomatic αS^{tg} mice were dissected within a few days after the onset of hindlimb paresis to prevent suffering for ethical reasons and to minimize temporal changes that might influence the results.

Biochemical Fractionation of Neural Tissues by Graded Extraction

The forebrain, brainstem, and spinal cord from $\alpha S^{tg}/S4^{+/+}$ or $\alpha S^{tg}/S4^{-/-}$ mice (5–16 m.o.) were dissected, weighed, and homogenized by sonication in 3 ml/g of buffer C (10 mM Tris-HCl [pH 7.6], 0.15 M NaCl, 1% Triton X-100, and protease inhibitors). The supernatant, after centrifugation at 15,000 × g at 4°C for 0.5 hr, was labeled as "Triton-soluble fraction." The pellet was sonicated and re-extracted with 1 ml/g of buffer D (10 mM Tris-HCl [pH 8.0], 0.15 M NaCl, 1% Triton X-100, 0.5% sodium deoxycholate, and 0.1% SDS) and fractionated by centrifugation at 15,000 × g at 4°C for 0.5 hr, and the supernatant was labeled as "SDS-soluble fraction." The pellet was dissolved by sonication and boiling in buffer E (3% SDS and 5% β-mercaptoethanol, 1 ml/g pellet), and the lysate was termed "SDS-insoluble fraction." The amounts proportional to the original brain weight were loaded on separate lanes and each fraction was analyzed by immunoblot.

In Vitro Sedimentation, Aggregation, and Phosphorylation Assays

The recombinant His_6-tagged mouse $Sept4^{54\ kDa}$ was prepared in Sf9 cells (Kinoshita et al., 2002). For recombinant mouse $Sept4^{48\ kDa}$, GST-fusion protein was expressed in *E.coli* with a plasmid, pGEX-6P (GE Healthcare Biosciences). After purification of GST-$Sept4^{48\ kDa}$ with glutathione-agarose beads, GST-PreScission protease (Roche) was added to the beads to cleave the GST tag and release untagged $Sept4^{48\ kDa}$. For sedimentation assay, 20 μl reactions of recombinant human αS (wild-type, 4 μg, BioMol), recombinant mouse $Sept4^{54\ kDa}$ (2 μg), and/or BSA (2 μg, Sigma) in PBS were incubated at 4°C for 16 hr. Each reaction was ultracentrifuged at 4°C at 440,000 × g for 30 min. The supernatants and the pellets were analyzed by SDS-PAGE/CBB. For self-aggregation and phosphorylation assays, recombinant human αS (A53T mutant, 100 μg, BioMol) was incubated in 100 μl reactions of 30 mM Tris-HCl (pH 7.5) and BSA (100 μg, Sigma) or recombinant $Sept4^{48\ kDa}$ (20 μg) at 37°C. For phosphorylation assays, 4 mM $MgCl_2$, 2 mM ATP, and CKII (500 U, New England Biolabs) were added. The reactions sampled at 0, 2, and 44 hr were analyzed by SDS-PAGE/CBB, and analyzed by immunoblot for αS or $pSer^{129}\alpha S$.

Supplemental Data

The Supplemental Data for this article can be found online at http://www.neuron.org/cgi/content/full/53/4/519/DC1/.

ACKNOWLEDGMENTS

We thank R. Takahashi, Y. Mizuno, T. Iwatsubo, and Y. Kaziro for suggestions and encouragements; V.M.-Y. Lee and J.Q. Trojanowski for

the generous gift of α-*synuclein*^{A53T} transgenic mice; D.R. Borchelt for the prion promoter; S. Yamada for the generation of *Sept4-Tg* mice; A. Kinoshita, Y. Fukazawa, and R. Shigemoto for technical advice; and A. Khundakar for critical reading of our manuscript. This study was supported in part by Special Coordination Funds for Promoting Science and Technology; Grants-in-Aid from MEXT of Japan, PRESTO from JST, and Takeda Science Foundation (to M.K.); a postdoctoral fellowship from JSPS; and a Grant from the Ichiro Kanehara Memorial Foundation (to M.I.).

Received: May 26, 2006
Revised: December 11, 2006
Accepted: January 10, 2007
Published: February 14, 2007

REFERENCES

Abeliovich, A., Schmitz, Y., Farinas, I., Choi-Lundberg, D., Ho, W.H., Castillo, P.E., Shinsky, N., Verdugo, J.M., Armanini, M., Ryan, A., et al. (2000). Mice lacking alpha-synuclein display functional deficits in the nigrostriatal dopamine system. Neuron *25*, 239–252.

Beites, C.L., Xie, H., Bowser, R., and Trimble, W.S. (1999). The septin CDCrel-1 binds syntaxin and inhibits exocytosis. Nat. Neurosci. *2*, 434–439.

Beites, C.L., Campbell, K.A., and Trimble, W.S. (2005). The septin Sept5/CDCrel-1 competes with alpha-SNAP for binding to the SNARE complex. Biochem. J. *385*, 347–353.

Chandra, S., Gallardo, G., Fernandez-Chacon, R., Schluter, O.M., and Sudhof, T.C. (2005). Alpha-synuclein cooperates with CSPalpha in preventing neurodegeneration. Cell *123*, 383–396.

Choi, P., Snyder, H., Petrucelli, L., Theisler, C., Chong, M., Zhang, Y., Lim, K., Chung, K.K., Kehoe, K., D'Adamio, L., et al. (2003). SEPT5_v2 is a parkin-binding protein. Brain Res. Mol. Brain Res. *117*, 179–189.

Dawson, T.M., and Dawson, V.L. (2003). Molecular pathways of neurodegeneration in Parkinson's disease. Science *302*, 819–822.

Dent, J., Kato, K., Peng, X.R., Martinez, C., Cattaneo, M., Poujol, C., Nurden, P., Nurden, A., Trimble, W.S., and Ware, J.A. (2002). A prototypic platelet septin and its participation in secretion. Proc. Natl. Acad. Sci. USA *99*, 3064–3069.

Dong, Z., Ferger, B., Paterna, J.C., Vogel, D., Furler, S., Osinde, M., Feldon, J., and Büeler, H. (2003). Dopamine-dependent neurodegeneration in rats induced by viral vector-mediated overexpression of the parkin target protein, CDCrel-1. Proc. Natl. Acad. Sci. USA *100*, 12438–12443.

Field, C.M., and Kellogg, D. (1999). Septins: cytoskeletal polymers or signalling GTPases? Trends Cell Biol. *9*, 387–394.

Fujishima, K., Kiyonari, H., Kurisu, J., Hirano, T., and Kengaku, M. (2007). Targeted disruption of Sept3, a heteromeric assembly partner of Sept5 and Sept7 in axons, has no effect on developing CNS neurons. J. Neurochem., in press.

Fujiwara, H., Hasegawa, M., Dohmae, N., Kawashima, A., Masliah, E., Goldberg, M.S., Shen, J., Takio, K., and Iwatsubo, T. (2002). alpha-Synuclein is phosphorylated in synucleinopathy lesions. Nat. Cell Biol. *4*, 160–164.

Giasson, B.I., Duda, J.E., Quinn, S.M., Zhang, B., Trojanowski, J.Q., and Lee, V.M. (2002). Neuronal alpha-synucleinopathy with severe movement disorder in mice expressing A53T human alpha-synuclein. Neuron *34*, 521–533.

Hall, P.A., Jung, K., Hillan, K.J., and Russell, S.E. (2005). Expression profiling the human septin gene family. J. Pathol. *206*, 269–278.

Hsu, S.C., Hazuka, C.D., Roth, R., Foletti, D.L., Heuser, J., and Scheller, R.H. (1998). Subunit composition, protein interactions, and structures of the mammalian brain sec6/8 complex and septin filaments. Neuron *20*, 1111–1122.

Hyman, S.E., Malenka, R.C., and Nestler, E.J. (2006). Neural mechanisms of addiction: The role of reward-related learning and memory. Annu. Rev. Neurosci. *29*, 565–598.

Ihara, M., Tomimoto, H., Kitayama, H., Morioka, Y., Akiguchi, I., Shibasaki, H., Noda, M., and Kinoshita, M. (2003). Association of the cytoskeletal GTP-binding protein Sept4/H5 with cytoplasmic inclusions found in Parkinson's disease and other synucleinopathies. J. Biol. Chem. *278*, 24095–24102.

Ihara, M., Kinoshita, A., Yamada, S., Tanaka, H., Tanigaki, A., Kitano, A., Goto, M., Okubo, K., Nishiyama, H., Ogawa, O., et al. (2005). Cortical organization by the septin cytoskeleton is essential for structural and mechanical integrity of mammalian spermatozoa. Dev. Cell *8*, 343–352.

Kahle, P.J., Neumann, M., Ozmen, L., Muller, V., Odoy, S., Okamoto, N., Jacobsen, H., Iwatsubo, T., Trojanowski, J.Q., Takahashi, H., et al. (2001). Selective insolubility of alpha-synuclein in human Lewy body diseases is recapitulated in a transgenic mouse model. Am. J. Pathol. *159*, 2215–2225.

Kinoshita, A., Kinoshita, M., Akiyama, H., Tomimoto, H., Akiguchi, I., Kumar, S., Noda, M., and Kimura, J. (1998). Identification of septins in neurofibrillary tangles in Alzheimer's disease. Am. J. Pathol. *153*, 1551–1560.

Kinoshita, A., Noda, M., and Kinoshita, M. (2000). Differential localization of septins in the mouse brain. J. Comp. Neurol. *428*, 223–239.

Kinoshita, M. (2006). Diversity of septin scaffolds. Curr. Opin. Cell Biol. *18*, 54–60.

Kinoshita, M., Kumar, S., Mizoguchi, A., Ide, C., Kinoshita, A., Haraguchi, T., Hiraoka, Y., and Noda, M. (1997). Nedd5, a mammalian septin, is a novel cytoskeletal component interacting with actin-based structures. Genes Dev. *11*, 1535–1547.

Kinoshita, M., Field, C.M., Coughlin, M.L., Straight, A.F., and Mitchison, T.J. (2002). Self- and actin-templated assembly of mammalian septins. Dev. Cell *3*, 791–802.

Kuhlenbaumer, G., Hannibal, M.C., Nelis, E., Schirmacher, A., Verpoorten, N., Meuleman, J., Watts, G.D., De Vriendt, E., Young, P., Stogbauer, F., et al. (2005). Mutations in SEPT9 cause hereditary neuralgic amyotrophy. Nat. Genet. *37*, 1044–1046.

LaVoie, M.J., Ostaszewski, B.L., Weihofen, A., Schlossmacher, M.G., and Selkoe, D.J. (2005). Dopamine covalently modifies and functionally inactivates parkin. Nat. Med. *11*, 1214–1221.

Lee, F.J., Liu, F., Pristupa, Z.B., and Niznik, H.B. (2001). Direct binding and functional coupling of alpha-synuclein to the dopamine transporters accelerate dopamine-induced apoptosis. FASEB J. *15*, 916–926.

Lee, K.H., Kim, M.Y., Kim, D.H., and Lee, Y.S. (2004). Syntaxin 1A and receptor for activated C kinase interact with the N-terminal region of human dopamine transporter. Neurochem. Res. *29*, 1405–1409.

Masuda, M., Dohmae, N., Nonaka, T., Oikawa, T., Hisanaga, S., Goedert, M., and Hasegawa, M. (2006). Cysteine misincorporation in bacterially expressed human alpha-synuclein. FEBS Lett. *580*, 1775–1779.

Miyakawa, T., Yamada, M., Duttaroy, A., and Wess, J. (2001). Hyperactivity and intact hippocampus-dependent learning in mice lacking the M1 muscarinic acetylcholine receptor. J. Neurosci. *21*, 5239–5250.

Moore, D.J., West, A.B., Dawson, V.L., and Dawson, T.M. (2005). Molecular pathophysiology of Parkinson's disease. Annu. Rev. Neurosci. *28*, 57–87.

Ono, R., Ihara, M., Nakajima, H., Ozaki, K., Kataoka-Fujiwara, Y., Taki, T., Nagata, K., Inagaki, M., Yoshida, N., Kitamura, T., et al. (2005). Disruption of Sept6, a fusion partner gene of Mixed Lineage Leukemia (MLL), does not affect the ontogeny, leukemogenesis induced by MLL-SEPT6, or the phenotype induced by the loss of Sept4. Mol. Cell. Biol. *25*, 10965–10978.

Peng, X.R., Jia, Z., Zhang, Y., Ware, J., and Trimble, W.S. (2002). The septin CDCrel-1 is dispensable for normal development and neurotransmitter release. Mol. Cell. Biol. *22*, 378–387.

Rekas, A., Adda, C.G., Andrew Aquilina, J., Barnham, K.J., Sunde, M., Galatis, D., Williamson, N.A., Masters, C.L., Anders, R.F., Robinson, C.V., et al. (2004). Interaction of the molecular chaperone alphaB-crystallin with alpha-synuclein: effects on amyloid fibril formation and chaperone activity. J. Mol. Biol. *340*, 1167–1183.

Shimura, H., Schlossmacher, M.G., Hattori, N., Frosch, M.P., Trockenbacher, A., Schneider, R., Mizuno, Y., Kosik, K.S., and Selkoe, D.J. (2001). Ubiquitination of a new form of alpha-synuclein by parkin from human brain: implications for Parkinson's disease. Science *293*, 263–269.

Son, J.H., Kawamata, H., Yoo, M.S., Kim, D.J., Lee, Y.K., Kim, S., Dawson, T.M., Zhang, H., Sulzer, D., Yang, L., et al. (2005). Neurotoxicity and behavioral deficits associated with Septin5 accumulation in dopaminergic neurons. J. Neurochem. *94*, 1040–1053.

Spiliotis, E.T., Kinoshita, M., and Nelson, W.J. (2005). A mitotic septin scaffold required for mammalian chromosome congression and segregation. Science *307*, 1781–1785.

Starke, K., Gothert, M., and Kilbinger, H. (1989). Modulation of neurotransmitter release by presynaptic autoreceptors. Physiol. Rev. *69*, 864–989.

Surka, M.C., Tsang, C.W., and Trimble, W.S. (2002). The mammalian septin MSF localizes with microtubules and is required for completion of cytokinesis. Mol. Biol. Cell. *13*, 3532–3545.

Tofaris, G.K., Razzaq, A., Ghetti, B., Lilley, K.S., and Spillantini, M.G. (2003). Ubiquitination of alpha-synuclein in Lewy bodies is a pathological event not associated with impairment of proteasome function. J. Biol. Chem. *278*, 44405–44411.

Versele, M., and Thorner, J. (2005). Some assembly required: yeast septins provide the instruction manual. Trends Cell Biol. *15*, 414–424.

Xue, J., Tsang, C.W., Gai, W.P., Malladi, C.S., Trimble, W.S., Rostas, J.A., and Robinson, P.J. (2004). Septin 3 (G-septin) is a developmentally regulated phosphoprotein enriched in presynaptic nerve terminals. J. Neurochem. *91*, 579–590.

Zhang, J., Forkstam, C., Engel, J.A., and Svensson, L. (2000a). Role of dopamine in prepulse inhibition of acoustic startle. Psychopharmacology (Berl.) *149*, 181–188.

Zhang, Y., Gao, J., Chung, K.K., Huang, H., Dawson, V.L., and Dawson, T.M. (2000b). Parkin functions as an E2-dependent ubiquitin-protein ligase and promotes the degradation of the synaptic vesicle-associated protein, CDCrel-1. Proc. Natl. Acad. Sci. USA *97*, 13354–13359.

Human Molecular Genetics, 2007, Vol. 16, No. 6 **678–690**
doi:10.1093/hmg/ddm013
Advance Accessed published on March 6, 2007

Leucine-rich repeat kinase 2 associates with lipid rafts

Taku Hatano[1], Shin-ichiro Kubo[1], Satoshi Imai[1], Masahiro Maeda[3], Kiyoshi Ishikawa[3], Yoshikuni Mizuno[2] and Nobutaka Hattori[1,2,*]

[1]Department of Neurology, [2]Research Institute for Diseases of Old Age, Juntendo University School of Medicine, 2-1-1 Hongo, Bunkyo, Tokyo 113-8421, Japan and [3]Immuno-Biological Laboratories Co., Ltd, 1091-1 Naka, Fujioka, Gunma 375-0005, Japan

Received November 7, 2006; Revised January 5, 2007; Accepted February 2, 2007

***Leucine-Rich Repeat Kinase 2* (*LRRK2*) is a causative gene for the autosomal dominant form of Parkinson's disease (PD). The gene encodes the ~280 kDa LRRK2 protein composed of domains such as leucine-rich repeats, Ras in complex proteins (Roc) followed by C-terminal of Roc (COR), mitogen-activated protein kinase kinase kinase (MAPKKK) and WD40. However, the normal function of the protein as well as its contribution to the pathogenesis of PD remains largely unknown. Here we describe the localization of LRRK2 in Golgi apparatus, plasma membrane and synaptic vesicles in cultured cells including mouse primary neurons. The membrane association of LRRK2 resists solubilization by ice-cold 1% Triton X-100, indicating its association through lipid rafts. To investigate whether mutations found in PD patients affect the localization of LRRK2, we transfected various LRRK2 mutants into cultured cells and performed fractionation experiments. Unexpectedly, the mutants are collected in both membrane and soluble fractions in a manner similar to wild type (WT). I2020T mutant LRRK2 associates with lipid rafts, similar to the WT. The lipid raft association of LRRK2 mutants as well as WT LRRK2 suggests that alteration of LRRK2 function on lipid rafts contributes to the pathogenesis of PD.**

INTRODUCTION

Parkinson's disease (PD) is one of the most common neurodegenerative diseases and is characterized by progressive dopaminergic neuronal loss. Genetic predisposition has been proposed recently as one of the major factors in the development of PD. Indeed, six causative genes have been identified as causes of the monogenic form of PD. Among them, missense mutations in the *leucine-rich repeat kinase 2* (*LRRK2*) gene have been found as the cause of autosomal dominant PD, one of the most common forms of familial PD (1–4). *LRRK2* gene encodes a large protein of 2527 amino acids (a.a.) with a molecular weight of ~280 kDa that contains leucine-rich repeats, Ras in complex proteins (Roc) followed by C-terminal of Roc (COR), mitogen-activated protein kinase kinase kinase (MAPKKK) and WD40 (5,6). Recent studies reported that LRRK2 protein exhibits kinase activity and that such activity is increased in its mutants (7,8). Consistently, increased kinase activity of the LRRK2 mutants induces neurotoxicity (9). LRRK2 has also been reported to localize to cytoplasmic structures such as mitochondria, Golgi apparatus, endoplasmic reticulum and cytoskeleton (7,8). However, there is little information on the normal function of LRRK2 and its role in the pathogenesis of PD. Since LRRK2 is implicated in the pathogenesis of PD in conjunction with both α-synuclein and tau proteins (2), characterization of LRRK2 should enhance our understanding of the pathomechanism of not only *LRRK2*-linked PD but also the sporadic form of disease.

In the present study, we used cultured cells including primary neurons from mouse brains to show the localization of LRRK2 in the Golgi apparatus, plasma membrane and synaptic vesicles. This membrane association of LRRK2 resists solubilization by ice-cold 1% Triton X-100, indicating that LRRK2 associates with lipid rafts, which are known to play important roles in cellular functions such as signal transduction, membrane trafficking and cytoskeletal organization (10). We also investigated the effects of mutations found in PD patients on the biochemical properties of LRRK2. Intriguingly, the mutants behave in a manner similar to the wild type (WT), with regard to association with membrane including

*Correspondence should be addressed. Tel: +81 338133111; Fax: +81 358000547; Email: nhattori@med.juntendo.ac.jp

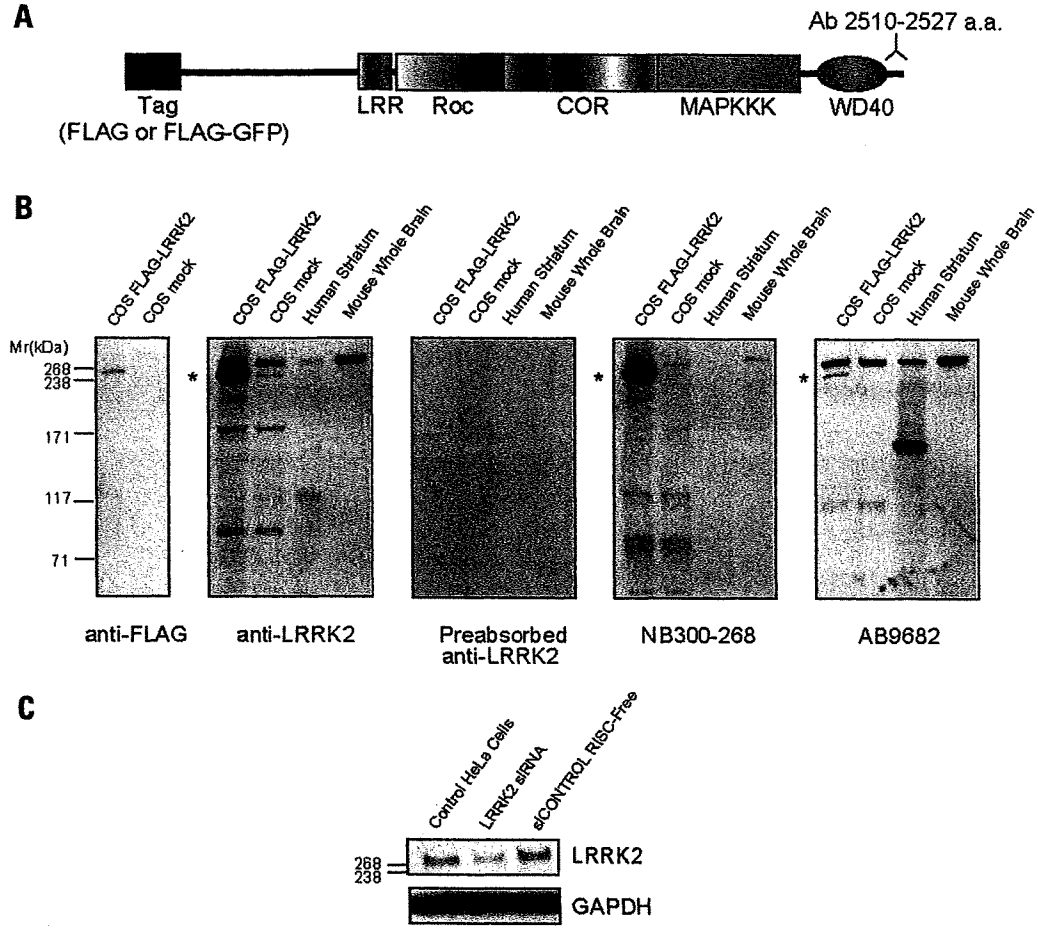

Figure 1. Characterization of polyclonal anti-LRRK2 antibodies. **(A)** Schematic representation of LRRK2 expression construct in vector. This construct was designed with FLAG or FLAG-GFP tag. We raised anti-LRRK2 antibody against 18 amino acids at C-terminus. **(B)** Western blot of COS-1 cells transfected with FLAG-LRRK2 or empty vector as a mock, human brain (striatum) and mouse whole brain probed with anti-FLAG, anti-LRRK2, and commercially available anti-LRRK2 (rabbit polyclonal antibodies; Novus Cat No. NB300-268 and Chemicon Cat No. AB9682) antibodies. Specificity of our antibody is confirmed by a pre-absorption test. Asterisk indicates overexpressed FLAG-LRRK2. **(C)** LRRK2 siRNA but not siCONTROL RISC-Free depresses endogenous LRRK2 protein as shown by western blot in HeLa cells. Equal volumes of each were then blotted for LRRK2 and GAPDH as an internal marker.

lipid rafts. The results suggest that LRRK2 mutants cause PD by inhibiting the normal function of WT or gain of function effects on lipid rafts.

RESULTS

Characterization of anti-LRRK2 antibody

To detect LRRK2, we first generated a rabbit polyclonal anti-LRRK2 antibody with synthetic peptides at just the C-terminal end (2510–2527 a.a.) of human LRRK2 (see: Materials and Methods section) (Fig. 1A). Western blot analysis using this antibody reveals several bands including a doublet of ~280 kDa, which correspond to the expected molecular size of LRRK2 in extracts of COS-1 cells, human striatum and mouse whole brains. All bands disappear when the antibody is preincubated with excess amount of the antigen, confirming the specificity of the antibody. The presence of multiple bands on western blot suggests that the protein is cleaved in the cells or during the process of cell lysis. On the other hand, western blot using FLAG antibody shows a single band of ~280 kDa, corresponding to the lower band of the doublet (asterisk, Fig. 1B) in lysates of COS-1 cells transfected with LRRK2 N-terminally fused with FLAG tag (FLAG-LRRK2). The difference in the molecular size between endogenous and transfected LRRK2 might indicate post-translational modification of endogenous LRRK2 or cleavage of transfected FLAG-LRRK2. In another control experiment, commercially available antibodies (rabbit polyclonal antibodies; Novus Cat No. NB300-268 and Chemicon Cat No. AB9682) also detect the enhanced lower band of the doublet in lysates of COS-1 cells transfected with FLAG-LRRK2, similar to our antibody, indicating the specificity of our antibody (Fig. 1B). To further confirm the specificity of our antibody, HeLa cells were transfected with short interference RNA (LRRK2 siRNA) to block endogenous LRRK2 RNA. As shown in Fig. 1C, the corresponding bands for LRRK2 are weaker, indicating that our antibody recognizes endogenous LRRK2. Immunocytochemistry for endogenous LRRK2 in COS-1 cells using anti-LRRK2 antibody shows punctate structures in the perinuclear region, which disappear when using preabsorbed antibody (Fig. 2A). The distribution

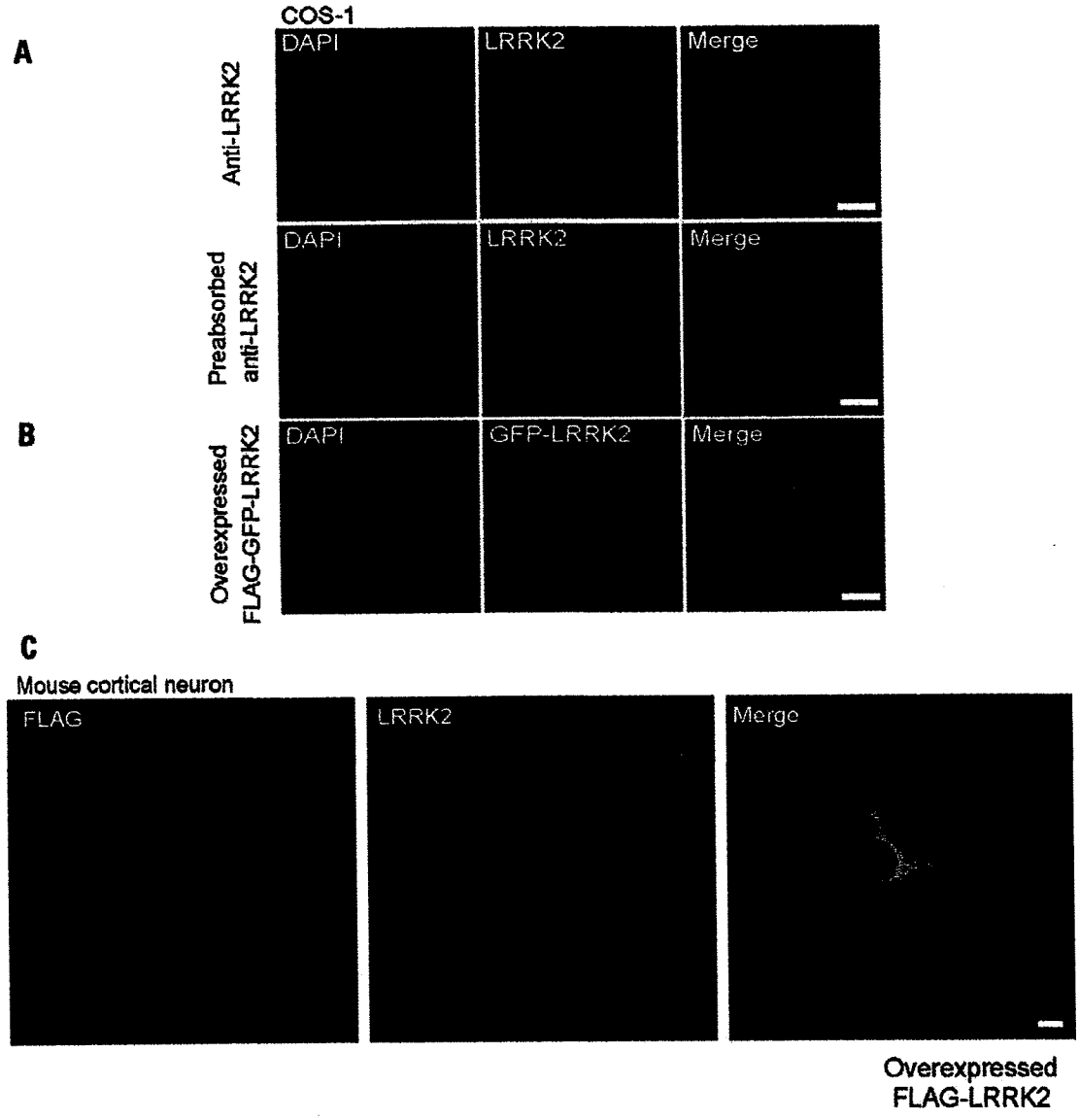

Figure 2. Anti-LRRK2 antibody recognizes endogenous and overexpressed LRRK2 in cultured cells. (**A**) Immunocytochemistry of COS-1 with anti-LRRK2 (top panel) and pre-absorbed anti-LRRK2 (bottom panel). LRRK2 immunoreactivity is recognized as large punctate structures in the perinuclear region. (**B**) Images of COS-1 cells transiently transfected with FLAG-GFP-LRRK2. The localization of FLAG-GFP-LRRK2 shows a pattern identical to that of endogenous LRRK2. (**C**) Immunocytochemistry of mouse primary cortical neurons transiently expressing FLAG-LRRK2 with anti-LRRK2 (green) and anti-FLAG (red) antibodies. Nuclei were stained blue with DAPI (A, B). Scale bars = 10 μm.

of fluorescence for FLAG-GFP-LRRK2 fusion protein overexpressed in COS-1 cells is also similar to that of endogenous LRRK2 (Fig. 2B). Furthermore, double staining with anti-LRRK2 and anti-FLAG antibodies is completely superimposed in a punctate appearance for FLAG-LRRK2 overexpressed in mouse cortical neurons, confirming the specificity of anti-LRRK2 antibody (Fig. 2C). These data indicate that our anti-LRRK2 antibody recognizes endogenous LRRK2 and was used in the following experiments.

LRRK2 localizes to the *trans*-Golgi network and cellular vesicles

To investigate the subcellular distribution of endogenous LRRK2, we double-stained COS-1 cells with anti-LRRK2 antibody and antibodies for several markers of intracellular organelles. LRRK2 largely colocalizes with γ-adaptin, a marker specific for *trans*-Golgi network (TGN), which is a subcompartment of the Golgi apparatus (11). In addition to the Golgi apparatus, LRRK2 also overlaps, though to a lesser extent, with the early endosomes (EEA1), lysosomes (LysoTracker) and mitochondria (MitoTracker) (Fig. 3A). To confirm the Golgi localization of LRRK2, we treated COS-1 cells with brefeldin A (BFA). BFA reversibly blocks the transfer of proteins from the endoplasmic reticulum to the Golgi apparatus and subsequently disrupts the structures of the Golgi apparatus (12). Treatment for COS-1 cells with BFA disperses the staining of LRRK2 as well as γ-adaptin from the perinuclear region to the cytoplasm, and washing out BFA from the medium results in recovery of the

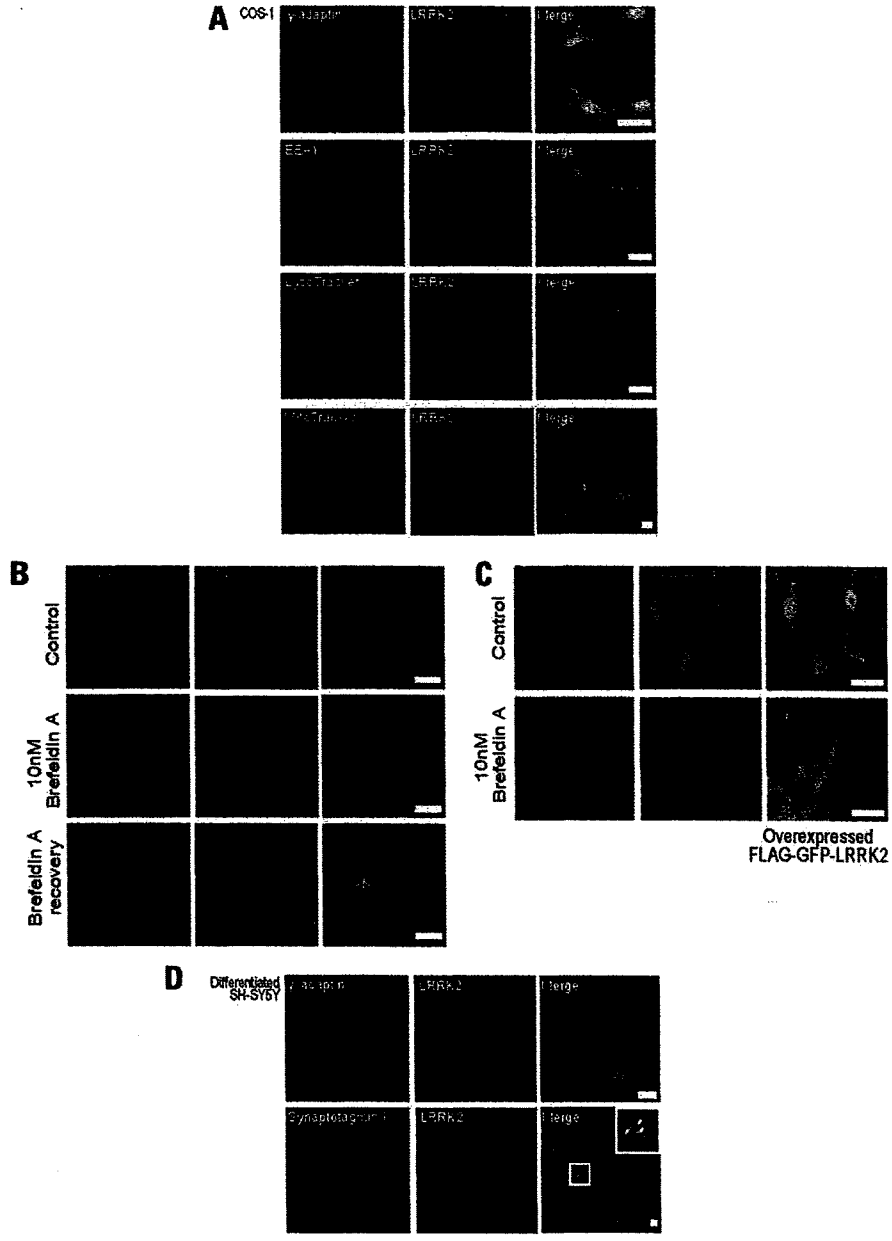

Figure 3. LRRK2 localized to Golgi apparatus and vesicles in COS-1 and SH-SY5Y cells. (**A**) COS-1 cells were fixed, permeabilized, immunostained for anti-LRRK2 antibody, and double-stained for anti-γ-adaptin (Golgi apparatus), anti-EEA1 (early endosomes), LysoTracker (lysosomes) and MitoTracker (mitochondria). (**B**) BFA treatment (middle panels) disperses both LRRK2 and γ-adaptin compared with control (top panels). This effect is reversible after BFA removal for 1 h (bottom panels). (**C**) Following treatment of COS-1 cells expressing FLAG-GFP-LRRK2 (green) with or without BFA, they were immunostained with γ-adaptin. In BFA-untreated cells, the FLAG-GFP-LRRK2 protein colocalizes with γ-adaptin. BFA treatment also disperses the localization of FLAG-GFP-LRRK2. (**D**) SH-SY5Y cells were treated with 10 nM retinoic acid for 7 days (differentiated SH-SY5Y) and then analyzed by double immunostaining with anti-γ-adaptin or anti-synaptotagmin I with anti-LRRK2 antibodies. LRRK2 localizes to Golgi apparatus and secretory vesicles (white arrows) in differentiated SH-SY5Y cells. All samples were examined with a LSM 510 confocal microscope and superimposed images (Merge) were produced to compare the staining pattern. Nuclei were stained blue with DAPI (A, C, D). Scale bars = 10 μm.

perinuclear localization of these proteins (Fig. 3B). In addition, we performed the same experiments using COS-1 cells transfected with FLAG-GFP-LRRK2 fusion protein and found that the protein behaves in a manner similar to endogenous LRRK2 with regard to localization and response to BFA (Fig. 3C). To further characterize subcellular localization of endogenous LRRK2 in neuronal cells, we performed double-labeling experiments using differentiated SH-SY5Y cells and revealed that LRRK2 colocalizes with γ-adaptin and synaptotagmin I, a major membrane protein of secretory vesicles budding from the TGN (Fig. 3C) (13–17). Since synaptotagmin I is transported on transporting organelles before reaching the nerve terminal (18,19), the colocalization of LRRK2 with synaptotagmin I in neurites (Fig. 3D; inset square) indicates that LRRK2 also travels from the TGN to the nerve terminal on organelles same as those of synaptotagmin I. These results

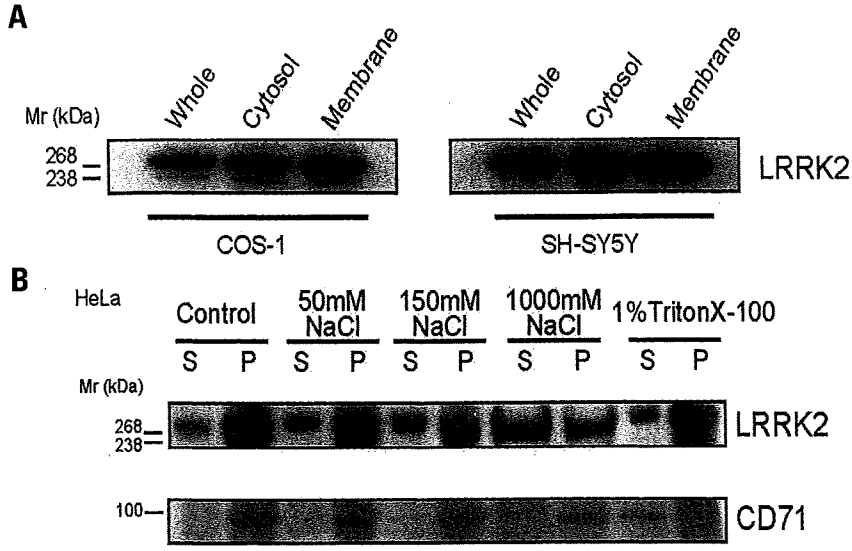

Figure 4. LRRK2 localizes at both cytosol and membrane. **(A)** LRRK2 is concentrated in both the cytosol and membrane fractions of COS-1 and SH-SY5Y cells. Cells were fractionated into whole, cytosol (100 000×*g* supernatant) and membrane (100 000 × *g* pellet) in detergent-free isotonic buffer. Aliquots of fractions, containing equal amounts of protein, were loaded and followed by immunoblotting. **(B)** Effects of various salt concentrations and non-ionic detergent on solubilization of LRRK2 and transferrin receptor (CD71). Increasing the salt concentration results in breaking off the connection with the membrane, whereas CD71 remains in the pellets. However, incubation with non-ionic detergent 1% Triton X-100, does not result in release of LRRK2 from the membrane. CD71 is readily solubilized in this condition. Equal volumes of each fraction were loaded, followed by immunoblotting.

suggest that LRRK2 associates with cellular membranes and localizes to intracellular organelles. To demonstrate the membrane association of LRRK2 biochemically, we fractionated COS-1 and SH-SY5Y cells into 100 K pellets and supernatants corresponding to membrane and cytosolic fractions, respectively. As shown in Fig. 4A, a significant amount of LRRK2 is collected in the membrane fraction, consistent with aforementioned results of immunocytochemistry.

LRRK2 has no obvious amino acid sequences for targeting signal and transmembrane domains based on computer analysis (20), yet it associates with cellular membranes. How could this happen? To address this question, we examined the effects of ionic strength on the association of LRRK2 with cellular membranes. Under low-salt conditions at neutral pH, LRRK2 is recovered mostly in the pellet. Increasing the salt concentration results in a considerable loss of LRRK2 from the membranes whereas transferrin receptor (CD71) remains in the pellets (Fig. 4B). These results indicate that LRRK2 is weakly associated with the surface of cellular membranes. To our surprise, LRRK2 does not dissociate from the membranes by solubilization with a non-ionic detergent Triton X-100 at 4°C, whereas CD71 is readily solubilized (Fig. 4B).

LRRK2 binds to detergent-resistant membranes

As stated above, the membrane association of LRRK2 resists solubilization by 1% Triton X-100 at 4°C (Fig. 4B). This finding suggests LRRK2 binding to lipid rafts. Lipid rafts are defined biochemically by their insolubility in ice-cold non-ionic detergent and they behave as low-density membranes during equilibrium sedimentation. To test whether LRRK2 binds to lipid rafts, we solubilized HeLa cells in 1% Triton X-100 at 4°C and separated the remaining membranes on a sucrose density gradient. Under these conditions, a substantial proportion of endogenous LRRK2 from HeLa cells associates with light membranes, and cofractionates with GPI-anchored protein CD55, a resident protein in lipid rafts (10,21–23) (Fig. 5A). As expected, CD71, which is known as a non-raft marker, remains soluble at the bottom fractions (Fig. 5A). Furthermore, disruption of lipid rafts by depletion of cholesterol with methyl-β-cyclodextrin (MBCD) eliminates the amount of LRRK2 in light membrane fractions. The amount of LRRK2 in lipid raft fractions (fractions no. 4–6), expressed as percentage of total LRRK2 protein, is 22.04 ± 9.90% under control and 0% under MBCD conditions (Fig. 5B). These results indicate that LRRK2 associates with lipid rafts. To visualize the association of LRRK2 with lipid rafts immunocytochemically, we double-stained HeLa cells for endogenous LRRK2 and markers for raft and non-raft membranes. Consistent with the results of the biochemical experiments, LRRK2 colocalized with raft markers such as G_{M1} and CD55, but not with non-raft marker CD71 (23) (Fig. 5C). G_{M1} and CD55 have generally been considered as markers on the plasma membrane (21,22,24). Thus, intracellular LRRK2 does not colocalize with G_{M1} and CD55, whereas LRRK2 in the cortex of the cells colocalized with these markers.

LRRK2 binds to lipid rafts of synaptic terminals

The association of LRRK2 with lipid rafts in cultured cells prompted us to determine whether LRRK2 associates with lipid rafts in the brain. For this purpose, we fractionated mouse brain extracts by differential centrifugation and analyzed the presence of LRRK2 in each fraction by western blot. LRRK2 is considerably present in the synaptosomal fraction (P2′) and cofractionated with NR1A and synaptophysin, indicating its localization in synaptic terminals, including

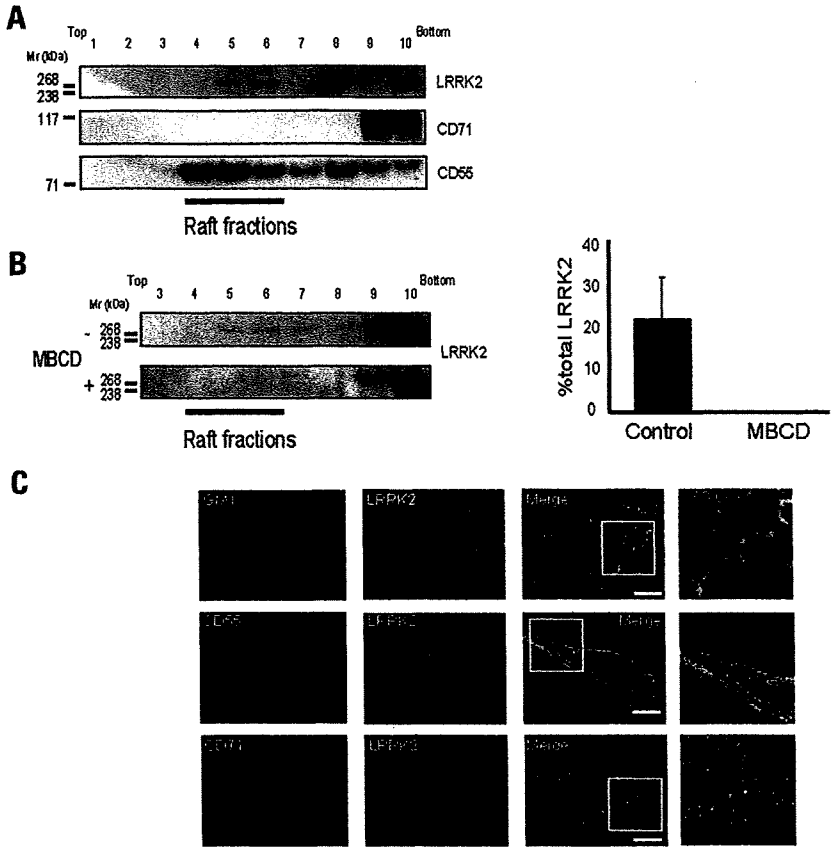

Figure 5. LRRK2 cofractionates with detergent-resistance membranes (**A**) HeLa cells were solubilized in 1% Triton X-100 at 4°C for 30 min, and extracts were separated by floatation through a sucrose density gradient. Endogenous LRRK2 comigrates with CD55 in light membrane fractions no. 4–6, whereas transferrin receptor (CD71) remains at the bottom fractions. (**B**) For depletion of cholesterol, cells were incubated with 20 mM methyl-β-cyclodextrin (MBCD) for 60 min at 37°C, solubilized in 1% Triton X-100 at 4°C and fractionated described as above. MBCD eliminates the membrane association of LRRK2 (bottom panel). Immunoreactivity was quantified and expressed as percentage of bound (fractions no. 4–6) to total LRRK2 protein. Data are the average ±SD of three independent experiments. (**C**) For staining the plasma membrane, cells were treated with mild fixation and permeabilization. The cells were double stained for LRRK2 and G_{M1}, CD55 (raft markers) and CD71 (non-raft marker). G_{M1} was detected using cholera toxin subunit B conjugated with Alexa-555. LRRK2 colocalizes extensively with G_{M1} and CD55 (top and middle panels) but not CD71 (bottom panel) of the plasma membrane. Scar bars = 10 μm (C).

synaptic plasma membranes (LP1) and synaptic vesicles (LP2). Intriguingly, we also identify LRRK2 signal in the soluble fraction of synaptic terminal (LS2) (Fig. 6A), again suggesting its weak association with the synaptic membranes.

Considering localization of LRRK2 in the synaptic membranes, we then investigated whether lipid rafts contribute to the membrane association of LRRK2 in synaptic terminals. For this purpose, we solubilized synaptosomes (P2′) in 1% Triton X-100 at 4°C and fractionated the resultant lysates by sucrose density gradient as described in Fig. 5A. LRRK2 cofractionates with GPI-anchored protein Thy-1.2, a raft-associated protein in neuronal cells (25). As expected CD71 which does not associate with lipid rafts remains soluble at the bottom of the gradient. Perturbation of the properties of lipid rafts by depletion of cholesterol with MBCD markedly reduces the amount of LRRK2 in light membrane fractions, indicating its association with lipid rafts of synaptic membranes. The amount of LRRK2 in lipid raft fractions (fractions no. 4–6), expressed as percentage of total LRRK2 protein, is 55.53 ± 16.49% under control and 25.55 ± 3.61% under MBCD conditions (Fig. 6B).

To visualize the association of LRRK2 with lipid rafts in neuronal cells, we double-stained mouse cortical neurons for LRRK2 and raft markers. Consistent with the results of biochemical experiments, LRRK2 colocalizes with raft markers such as Thy-1.2, G_{M1}, and phosphatidylinositol 4,5-bisphosphate (PIP_2) (10,23,26,27) (Fig. 7). We also analyzed subcellular localization of LRRK2 in mouse primary cultured neurons. In consistent with the data in Fig. 3D, LRRK2 colocalizes with synaptotagmin I in the processes of mouse striatal neurons, indicating its association with synaptic vesicles. In addition, we found perinuclear localization of LRRK2 costained with γ-adaptin in mouse cortical neurons (Fig. 7).

Pathogenic mutations do not disrupt LRRK2-lipid rafts interaction

We examined various LRRK2 mutants identified in patients for their abilities to associate with the membranes. Subcellular fractionation of COS-1 cells transfected with FLAG-tagged mutants shows that all of fusion proteins are mainly collected

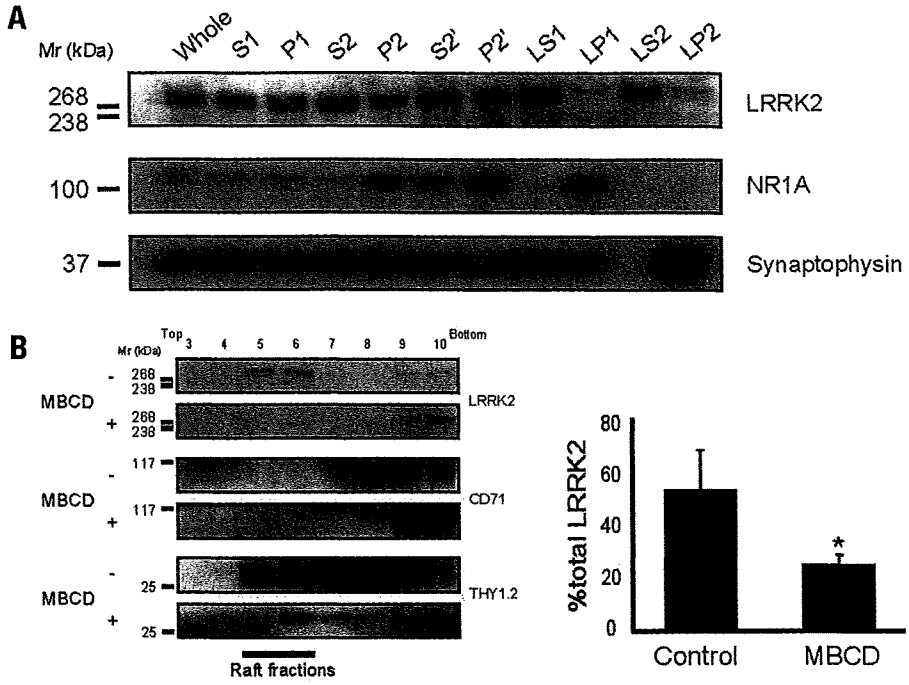

Figure 6. LRRK2 associates with lipid rafts at synaptic membranes in mouse brain. (**A**) LRRK2 concentrates in various subcellular fractions in mouse brain. Subcellular fractions obtained are designed as described in Methods. Aliquots of fractions, containing equal amounts of protein, were subjected to SDS-PAGE followed by immunoblotting with anti-LRRK2, anti-NR1A and anti-synaptophysin antibodies. (**B**) Mouse brain synaptosomes (P2' fraction) were untreated (MBCD-) or pretreated (MBCD+) for 1 h with 15 mM methyl-β-cyclodextrin (MBCD), then extracted with 1% Triton X-100 at 4°C and separated by floatation through sucrose gradients. Equal volumes of every fraction were subjected to SDS-PAGE followed by immunoblotting with anti-LRRK2, anti-Thy-1.2 (raft marker) and anti-transferrin receptor (CD71: non-raft marker) antibodies. LRRK2 is solubilized from lipid raft fractions and is shifted to soluble fractions of the gradient after MBCD+. Immunoreactivity was quantified and expressed as percentage of bound (fractions no. 4–6) to total LRRK2 protein. Data are the average ± SD of three independent experiments. $^*P < 0.05$; Student's *t*-test.

in the membrane fractions. There are no significant differences in the distribution patterns between WT and these mutants (Fig. 8A).

To further analyze the association of pathogenic LRRK2 mutants with lipid rafts, COS-1 cells were transfected with I2020T mutant as well as WT LRRK2 as a control. Transfected cells were solubilized with Triton X-100 at 4°C and then separated on a floatation gradient. Unexpectedly, the mutant LRRK2 floats up to the light membrane fraction, similar to WT. The amount of LRRK2 in lipid raft fractions (fractions no. 4–6), expressed as percentage of total LRRK2 protein, is 23.81 ± 10.03% in WT and 25.29 ± 7.93% in I2020T-transfected cells (Fig. 8B). Furthermore, we examined the effect of mutant using mouse primary cortical neurons transfected with FLAG-tagged WT and I2020T LRRK2. Confocal microscopic analyses reveal that both the WT and I2020T mutant LRRK2 colocalize with synaptotagmin I and PIP_2 (Fig. 8C). These results indicate that mutations in LRRK2 alter neither its subcellular localization nor its association with lipid rafts.

DISCUSSION

In the present study, we found that LRRK2 associates with cellular membranes using confocal microscopy and biochemical analysis in COS-1, HeLa, mouse primary neuronal cells and mouse synaptosomes. Immunofluorescence studies using anti-LRRK2 antibody reveal that the labeled structures represent not only diffuse cytoplasmic but also punctate distribution. Therefore, we performed double immunostaining studies to determine the subcellular localization of endogenous LRRK2 and found it localizes to the Golgi apparatus, cellular vesicles and plasma membrane in cultured cells. Cell fractionation studies reveal that LRRK2 is present in both soluble and membrane fractions. We also obtained similar results using cells that overexpressed FLAG- or FLAG-GFP-tagged LRRK2.

It is important to elucidate the precise subcellular localization of LRRK2 to understand the normal function of the protein as well as its role in the pathogenesis of LRRK2-linked PD. West *et al.* (7) reported that LRRK2 localizes in the cytoplasm and mitochondria in transiently transfected HEK293T cells. In addition, they also used fractionation assay to demonstrate the localization of LRRK2 to the outer membrane of mitochondria (7). We also found that although endogenous LRRK2 colocalizes in part with MitoTracker, which is a mitochondrial marker, it associates mostly with other membrane structures. Our results indicate that LRRK2 associates with cellular membrane structures, such as Golgi apparatus. This finding is consistent with that of a previous study (8). In addition, we demonstrate that LRRK2 also associates with early endosomes and lysosomes. However, LRRK2 is mainly identified in the Golgi apparatus, synaptic vesicles and plasma membrane rather than lysosomes and mitochondrial localization. In this regard, Biskup *et al.* (28)

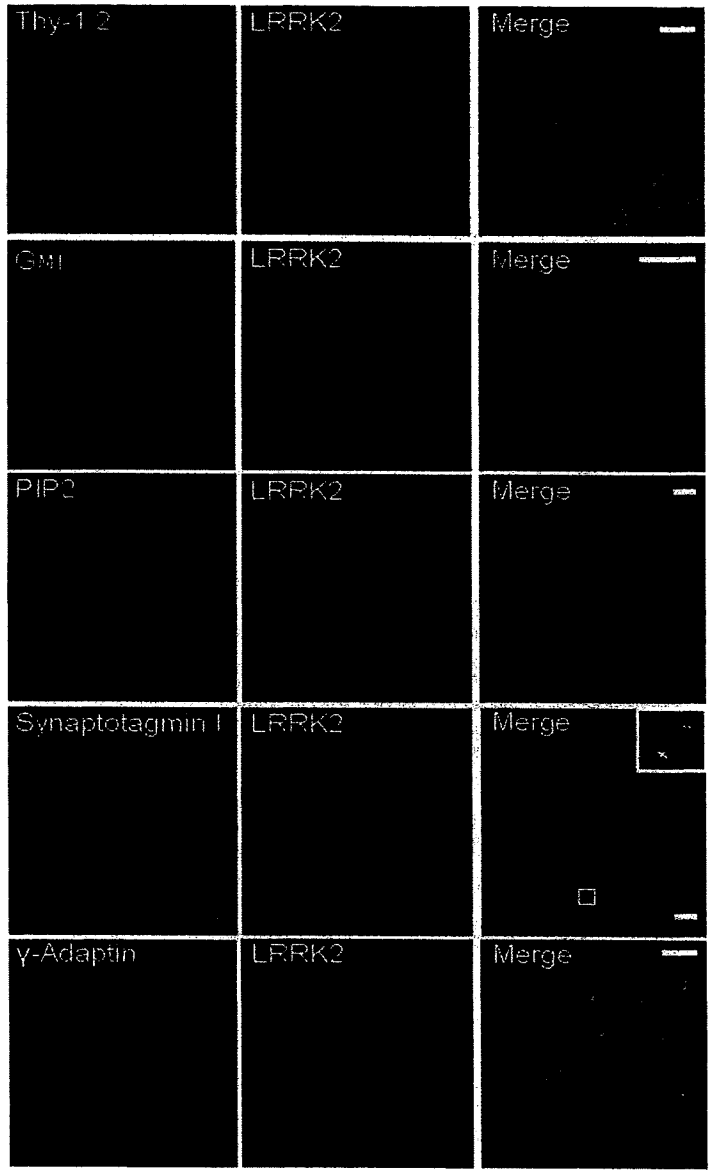

Figure 7. LRRK2 associates with lipid rafts and TGN in mouse cortical and striatal primary neurons. Primary cortical neurons were grown on coverslips. After mild fixation and permeabilization, the cells were double-stained for LRRK2 and Thy-1.2, G_{M1}, PIP_2 (raft markers), synaptotagmin I (vesicle marker) and γ-adaptin (Golgi marker). G_{M1} was detected using cholera toxin subunit B conjugated to Alexa-555. LRRK2 colocalizes extensively with raft components and Golgi marker. Arrows point to endogenous LRRK2 localized at synaptotagmin I-positive punctate structures. Scar bars = 10 μm.

demonstrated recently the association of LRRK2 with membrane structures such as lysosomes, endosomes, transport vesicles and mitochondria, consistent with our results. This characteristic distribution of LRRK2 could indicate that LRRK2 is involved in membrane trafficking system. In this context, LRRK2 could also contribute to vesicular transport system. Notably, LRRK2 fractionates with 1% Triton X-100-insoluble, light membrane and colocalizes with G_{M1}, PIP_2 and GPI-anchored protein such as CD55 and Thy-1.2. These results indicate that LRRK2 associates with lipid rafts, microdomains on the cellular membrane, which is rich in cholesterol, sphingomyelin, and phospholipids with saturated long chain fatty acids (29). Lipid rafts are involved in membranous organelles, e.g. Golgi apparatus, endoplasmic reticulum, plasma membrane, synaptic vesicles, mitochondria (30–33) and selectively incorporate or exclude proteins and thereby govern protein–protein and protein–lipid interactions (34). Lipid rafts play important roles *per se* in various cellular functions such as signal transduction, cytoskeletal organization and membrane trafficking including endocytosis and exocytosis (10,35,36). Considering the binding potentials of LRRK2 to lipid rafts at synaptic terminals, LRRK2 could be involved in the vesicular trafficking system such as exocytosis and endocytosis. Further support for the involvement of LRRK2 in vesicular trafficking system is provided by the presence of the ROC domain in LRRK2 similar in sequence to that of Rab family proteins (6), which are known to participate in exocytosis and endocytosis in conjunction with vesicle

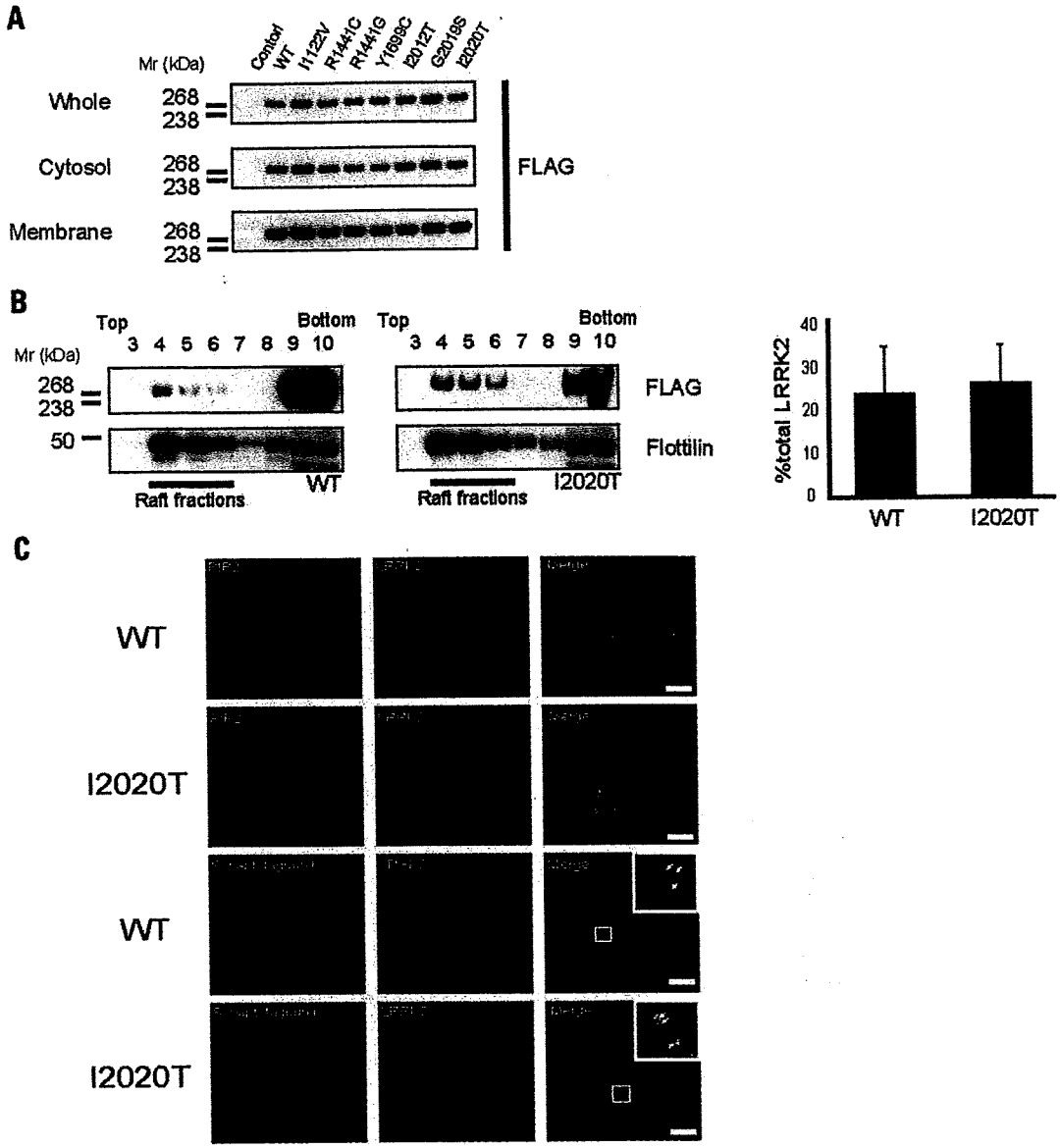

Figure 8. Pathogenic LRRK2 mutants do not alter localization and association with lipid rafts. (**A**) COS-1 cells were transfected with various mutants of FLAG-LRRK2, and lysates were separated into cytosolic and membrane fractions. Aliquots of each fraction, which contained equal amounts of protein, were subjected to western blot with anti-FLAG antibody. (**B**) COS-1 cells were transfected with WT and pathogenic mutant I2020T (I2020T), and extracted with 1% Triton X-100 at 4°C and separated by floatation through sucrose gradients. Equal volumes of each fraction were subjected to SDS-PAGE followed by immunoblotting with anti-FLAG antibody. Immunoreactivity was quantified and expressed as percentage of bound (fractions no. 4–6) to total LRRK2 protein. Data are the average ± SD of three independent experiments. (**C**) Primary neuronal cells were transfected with FLAG-GFP tagged WT and I2020T-LRRK2, immunolabeled for PIP_2 (raft marker) or synaptotagmin I (vesicle marker). Arrows point to WT and I2020T LRRK2 localized at synaptotagmin I-positive punctate structures. Pathogenic mutants did not alter the localization of WT. Scale bars = 10 μm (C).

formation, organelle motility and tethering of vesicles to target membrane (37). In addition, a kinase domain in LRRK2, known as MAPKKK, belongs to tyrosine kinase-like group (6) and one of which, the Raf/MAPK pathway, is activated within the lipid rafts when cells were infected with Coxsackievirus A9 (38). Epidermal growth factor (EGF)-dependent activation of Ras and MAPK pathway are also initiated in lipid rafts (39). Moreover, lipid rafts associate with SNARE proteins and regulate endocytosis and exocytosis (30,40,41). Thus, it is possible that LRRK2 interacts dynamically with lipid rafts and functions as a related molecule in vesicular trafficking system. Interestingly, MacLeod *et al.* (42) reported that LRRK2 regulates the maintenance of neurite process morphology in mammalian brains. Considering the localization of LRRK2 in lipid rafts, it is possible that LRRK2 plays an important role in axon guidance during development (43).

To clarify how LRRK2 mutants contribute to the pathogenesis of *LRRK2*- linked PD, we compared the subcellular localization and lipid rafts association in WT LRRK2 and mutants. Surprisingly, the pattern of subcellular localization and lipid raft association is quite similar in WT and mutants, suggesting that LRRK2 mutants disrupt the normal function of WT on the

lipid rafts as dominant negative effect or toxic-gain-of-function. This scenario is consistent with the inheritance mode of autosomal dominant fashion.

Although pathomechanism of PD remains unknown, a single gene defect must induce the nigral degeneration in familial PD. Accordingly, we hypothesize that familial PD-related gene products could share a common pathway. Indeed, α-synuclein and parkin are shown to associate with synaptic membranes (44–46) and their animal models exhibit altered synaptic functions (47–49). Intriguingly, both proteins have been shown to associate with lipid rafts (23,46,50). Therefore, these proteins as well as LRRK2 could be implicated in a common cascade of nigral degeneration. Indeed, parkin interacts with α-synuclein (51) and LRRK2 (52). PINK1, a protein responsible for an autosomal recessive form of PD (53,54), also resists various detergents and could associate with lipid rafts (55). These proteins could associate with each other at lipid rafts and perturbation of their interaction as well as lipid raft association might induce neuronal degeneration in PD. Understanding the physiological interactions between these proteins at lipid rafts may provide insights into the mechanism of neuronal degeneration and therapeutic approaches in PD.

MATERIALS AND METHODS

Antibodies and plasmids

FLAG (M2, HRP-M2, polyclonal) and γ-adaptin (mouse monoclonal) were purchased from Sigma-Aldrich (St Louis, MO). Monoclonal antibodies to Flotillin-1 (mouse), EEA1 (mouse), Thy-1.2 (rat) and NMDAR1 (mouse) were purchased from BD Biosciences Pharmingen (San Diego, CA). Rabbit polyclonal antibody to CD-55 (used for immunoblotting) was purchased from Santa Cruz Biotechnology (Santa Cruz, CA). Monoclonal antibodies to synaptophysin (mouse), transferrin receptor (CD71; mouse), CD55 (for immunocytochemistry; mouse), PIP_2 (mouse) and synaptotagmin I (mouse) were purchased from Progen Biotechnik (Heidelberg, Germany), Invitrogen-Molecular Probes (Eugene, OR), EMD Biosciences-Calbiochem (Darmstadt, Germany), Assay design (Ann Arbor, MI) and Wako Pure Chemical Industries (Osaka, Japan), respectively. Two types of rabbit polyclonal anti-LRRK2 antibodies were purchased from Chemicon International Inc. (Temecula, CA) and Novus Biologicals, Inc. (Littleton, CO). Secondary antibodies conjugated to horseradish peroxidase were purchased from GE HealthCare Bio-Sciences (Piscataway, USA) and Alexa 488, 568 and 594 conjugated secondary antibodies were from Invitrogen-Molecular Probes. A polyclonal antibody to human LRRK2 was raised by immunizing rabbits with synthetic peptides at C terminal 18 a.a. (HIEVRKELAEKMRRTSVE). Anti-serum was affinity-purified on columns against synthetic peptides. The pRK5-FLAG-LRRK2 vector (in-frame fusion of full-length LRRK2 at the C-terminus of FLAG tag) was a kind gift from Drs Hanafusa, Matsumoto (Nagoya University) and Shibuya (Tokyo Medical and Dental University). The vector was digested with *Bam*HI at the site between FLAG tag and LRRK2, and then a GFP tag was inserted (FLAG-GFP-LRRK2) (Fig. 1A). To generate LRRK2 mutant vectors, the QuikChange site-directed mutagenesis kit (Stratagene; La Jolla, CA) was used at provided condition. The amino acid sequence of each vector was compared with the current Entrez database entry for LRRK2 (accession No. AY792511).

Cell culture

COS-1, HeLa and SH-SY5Y cells were grown in Dulbecco's modified Eagle's medium (Sigma-Aldrich) with 10% fetal bovine serum (FBS; Sigma-Aldrich) and 1% penicillin-streptomycin (PS; Invitrogen-GIBCO) at 37°C and 5% CO_2. To induce cell differentiation, SH-SY5Y cells were incubated in complete medium plus 10 μM retinoic acid (Sigma-Aldrich) for 2 weeks. Primary cortical and striatum neuronal cells containing glia cells were prepared from E15.5 C57B6J mice and cultured on Fisherbrand 'coverglass for growth' (Fisher Scientific, Pittsburgh, USA) in starting medium (F12 and minimum essence medium with 10% FBS, 1% PS, and 0.001% insulin) for 3 days, incubated sequentially with 0.5 μM Ara-C (Sigma-Aldrich) in maintenance medium (F12 and minimum essence medium with 5% calf serum, 5% horse serum, 1% PS, and 0.001% insulin) for 5 days. When indicated, cells were transfected by using Lipofectamine™ 2000 (Invitrogen) at indicated conditions.

RNA interference

HeLa cells were transfected with siRNAs using Lipofectamine™ 2000 at indicated conditions. LRRK2 knockdown was achieved using LRRK2 siRNA (sense siRNA: 5′-CAAUGUCAGGUGUUAUAAUAU-3′), and a siCONTROL RISC-Free (a commercial base non-silencing siRNA) (Dharmacon Inc., Chicago, IL) was used as control.

Immunocytochemistry

Cells were fixed for 10 min in 4% paraformaldehyde (PFA) in phosphate-buffered saline (PBS), permeabilized with PBS containing 0.2% Triton X-100 (Sigma-Aldrich) for 5 min on ice. After blocking (1× BlockAce; Yukijirushi Co.) for 30 min, cells were incubated overnight with primary antibodies at 4°C, then incubated for 1 h with secondary antibodies and 1 nM of 6-diamidino-2-phenylindole (DAPI; Sigma-Aldrich) at room temperature. At the time of staining detergent-resistant membrane, cells were fixed for 5 min in 4% PFA and permeabilized with 0.02% Triton X-100 on ice. When indicated, cells were incubated for 30 min at 37°C with MitoTracker Red CMXRos or LysoTracker RedDND-99 (Invitrogen-Molecular Probes) in complete medium before fixation. To stain G_{M1}, cells were incubated for 30 min at 4°C with Vybrant Alexa Fluor 555 (Invitrogen-Molecular Probes). Slides were mounted with Vectashield (Vector Laboratories, Burlingame, CA) and analyzed by using Zeiss LSM 510 confocal microscopy.

Cell fractionation

For cell fractionation studies, cultured cells (COS-1, SH-SY5Y, HeLa) were washed three times with PBS,

scraped and centrifuged at 400×*g* for 5 min. Cell pellets were resuspended in homogenization buffer (20 mM HEPES pH 7.2, and 0.25 M sucrose) in the presence of a cocktail of protease inhibitors (Complete Mini, EDTA-free; Roche, Boehringer Mannheim), and sonicated at 4°C (10 s three times). The nuclei and unbroken cells were then pelleted by centrifugation at 1000×*g* for 10 min. The supernatant was centrifuged at 100 000×*g* for 1 h at 4°C to separate cytosolic and membrane fractions. For the study of effects of salts and non-ionic detergent on the solubilization of LRRK2, the membrane fraction was resuspended for 30 min with homogenization buffer with 50, 150 and 1000 mM sodium chloride or 1% Triton X-100 on ice. After separation of soluble and insoluble materials by centrifugation, equal volumes of each fraction were subjected to western blot with anti-LRRK2 and anti-CD71 antibodies.

Preparation of synaptic vesicles from mouse brain

The experimental protocol was approved by the Ethics Review Committee for Animal Experimentation of Juntendo University School of Medicine. Synaptic vesicles were prepared as described previously (45,56), with minor modification. Briefly, myelin-rich medulla oblongata was removed from brains of two mice, and placed into 9 ml ice-cold synaptosome homogenizing buffer (320 mM sucrose and 4 mM HEPES, pH 7.4) with Complete Mini, EDTA-free and phosphatase inhibitor cocktails I and II (Sigma-Aldrich). Tissues were homogenized using glass-Teflon homogenizer (12 up and down stroked, 900 r.p.m.). The homogenized brain sample was centrifuged for 15 min at 1000×*g*. The pellet (P1) was discarded, while the supernatant (S1) was centrifuged for 15 min at 12 000×*g*. The supernatant (S2) was removed and the pellet (P2) was washed with synaptosome homogenizing buffer, and then centrifuged for 15 min at 13 000×*g*. After removal of the supernatant (S2′), the pellet (P2′) was collected as crude synaptosome. P2' was subsequently resuspended with the synaptosome homogenizing buffer to yield a final volume of 600 μl, then 5.4 ml of ice cold distilled water was added with Complete Mini, EDTA-free. The samples were immediately subjected to five up-and-down strokes at 1200 r.p.m. and mixed with 50 μL 1M HEPES, pH 7.4, then centrifuged for 20 min at 33 000×*g* to yield the lysate pellet (LP1) and lysate supernatant (LS1). The supernatant was centrifuged for 2 h at 260 000×*g*. The supernatant (LS2) was removed and the pellet (LP2) was resuspended with 300 μl of the synaptosome homogenizing buffer. To loosen the pellet, samples were extruded consecutively through a 23-gauge and a 26-gauge hypodermic needle attached to a 1 ml syringe. The concentration of protein in each fraction was calculated by BCA protein assay kit (Pierce, Rockford, IL). Finally, 10 μg proteins from each fraction were analyzed by SDS-PAGE followed by immunoblotting.

Isolation of detergent-resistant membranes (DRMs)

DRMs were isolated from COS-1 cells, HeLa cells and mouse crude synaptosomes as described previously (23,50). Briefly, samples of cultured cells or crude synaptosomes were resuspended in DRMs lysis buffer (25 mM MES, pH 6.5, 50 mM NaCl, 1 mM NaF, 1 mM Na_3VO_4 and 1% Triton X-100) with Complete Mini, EDTA-free and phosphatase inhibitor cocktails I and II. Samples were incubated on ice for 30 min with Dounce homogenization every 10 min. The lysate was adjusted to 42.5% sucrose, overlaid with 35 and 5% sucrose in lysis buffer without detergent and ultracentrifuged at 275 000×*g* for 18 h. Ten fractions were collected from top to bottom. Equal volumes of each fraction were analyzed by western blot. For quantitative western blot, protein bands were quantified using ImageJ software (http://rsb.info.nih.gov/ij/). The amount of LRRK2 immunoreactivity in raft fractions (fractions no. 4–6) was expressed as percentage of the sum of LRRK2 immunoreactivity in every fraction. Differences between fractions were tested for statistical significance by using the Student's *t*-test.

To deplete cholesterol, HeLa cells and mouse synaptosomes were treated with MBCD (Sigma-Aldrich) as described previously (23,25). HeLa cells were starved for 2 h in serum-free medium and incubated for 1 h at 37°C in 20 mM MBCD. Mouse synaptosomal preparations (P2′) were treated for 1 h at 37°C in sodium buffer (10 mM glucose, 5 mM KCl, 140 mM NaCl, 5 mM $NaHCO_3$, 1 mM $MgCl_2$, 1.2 mM Na_2HPO_4 and 20 mM HEPES, pH 7.4) with Complete Mini, EDTA-free, phosphatase inhibitor cocktails I and II and 15 mM MBCD (25). After depletion of cholesterol, lipid rafts were obtained as described above.

Immunoblotting

Cell lysates were mixed with Laemmli sample buffer and incubated at room temperature for 2 h. The samples were resolved on 3–8% NuPAGE Tris-Acetate polyacrylamide gels (Invitrogen) in 1 × NuPAGE Tris-acetate running buffer and transferred onto polyvinylidene fluoride (PVDF) membrane (Bio-Rad Bioscience; Hercules, CA). The membranes were blocked for 1 h in PBS containing 0.05% Tween-20 (PBS-T) and 5% non-fat milk (BD Difco) and then incubated overnight at 4°C with the primary antibody. The membranes were washed with PBS-T four times followed by incubation for 1 h at room temperature with horseradish peroxidase-conjugated anti-mouse, rabbit and rat IgG (1:2000 dilution) and immunoreactivity assessed by chemiluminescence reaction using ECL plus reagent (GE Health Care Bio-Sciences) or Western Lightning (Perkin Elmer-Cetus, Foster City, CA).

ACKNOWLEDGEMENTS

We thank Manabu Funayama, Takeo Arai, Kahori Shiba, Yoko Chikaoka-Kawamura, Norihiro Tada, Yuanzhe Li, Osamu Imamura, Hiromi Kaneko-Fujimoto and Yoko Imamichi (Juntendo University). We are grateful to Venu M. Nemani (University of California, San Francisco) for technical advice. We also thank Hiroshi Hanafusa, Kunihiro Matsumoto (Nagoya University) and Hiroshi Shibuya (Tokyo Medical and Dental University) for providing pRK5-FLAG-LRRK2 vector. This study was supported by grants from the Ministry of Education, Science, Sports and Culture of Japan, and by the Fund for 'Research for the Future' program from the Japan Society for the Promotion of Science.

Conflict of Interest statement. The authors declare no conflict of interest.

REFERENCES

1. Paisan-Ruiz, C., Jain, S., Evans, E.W., Gilks, W.P., Simon, J., van der Brug, M., Lopez de Munain, A., Aparicio, S., Gil, A.M., Khan, N. *et al.* (2004) Cloning of the gene containing mutations that cause PARK8-linked Parkinson's disease. *Neuron*, **44**, 595–600.
2. Zimprich, A., Biskup, S., Leitner, P., Lichtner, P., Farrer, M., Lincoln, S., Kachergus, J., Hulihan, M., Uitti, R.J., Calne, D.B. *et al.* (2004) Mutations in LRRK2 cause autosomal-dominant parkinsonism with pleomorphic pathology. *Neuron*, **44**, 601–607.
3. Funayama, M., Hasegawa, K., Ohta, E., Kawashima, N., Komiyama, M., Kowa, H., Tsuji, S. and Obata, F. (2005) An LRRK2 mutation as a cause for the parkinsonism in the original PARK8 family. *Ann. Neurol.*, **57**, 918–921.
4. Tomiyama, H., Li, Y., Funayama, M., Hasegawa, K., Yoshino, H., Kubo, S.I., Sato, K., Hattori, T., Lu, C.S., Inzelberg, R. *et al.* (2006) Clinicogenetic study of mutations in LRRK2 exon 41 in Parkinson's disease patients from 18 countries. *Mov. Disord.*, **21**, 1102–1108.
5. Mata, I.F., Wedemeyer, W.J., Farrer, M.J., Taylor, J.P. and Gallo, K.A. (2006) LRRK2 in Parkinson's disease: protein domains and functional insights. *Trends Neurosci.*, **29**, 286–293.
6. Marin, I. (2006) The Parkinson Disease gene LRRK2: evolutionary and structural insights. *Mol. Biol. Evol.*, **23**, 2423–2433.
7. West, A.B., Moore, D.J., Biskup, S., Bugayenko, A., Smith, W.W., Ross, C.A., Dawson, V.L. and Dawson, T.M. (2005) Parkinson's disease-associated mutations in leucine-rich repeat kinase 2 augment kinase activity. *Proc. Natl. Acad. Sci. USA*, **102**, 16842–16847.
8. Gloeckner, C.J., Kinkl, N., Schumacher, A., Braun, R.J., O'Neill, E., Meitinger, T., Kolch, W., Prokisch, H. and Ueffing, M. (2006) The Parkinson disease causing LRRK2 mutation I2020T is associated with increased kinase activity. *Hum. Mol. Genet.*, **15**, 223–232.
9. Smith, W.W., Pei, Z., Jiang, H., Dawson, V.L., Dawson, T.M. and Ross, C.A. (2006) Kinase activity of mutant LRRK2 mediates neuronal toxicity. *Nat. Neurosci.*, **9**, 1231–1233.
10. Brown, D.A. and London, E. (1998) Functions of lipid rafts in biological membranes. *Annu. Rev. Cell Dev. Biol.*, **14**, 111–136.
11. Ahle, S., Mann, A., Eichelsbacher, U. and Ungewickell, E. (1988) Structural relationships between clathrin assembly proteins from the Golgi and the plasma membrane. *EMBO J.*, **7**, 919–929.
12. Dinter, A. and Berger, E.G. (1998) Golgi-disturbing agents. *Histochem. Cell Biol.*, **109**, 571–590.
13. Orci, L., Ravazzola, M., Amherdt, M., Perrelet, A., Powell, S.K., Quinn, D.L. and Moore, H.P. (1987) The *trans*-most cisternae of the Golgi complex: a compartment for sorting of secretory and plasma membrane proteins. *Cell*, **51**, 1039–1051.
14. Tooze, S.A. and Huttner, W.B. (1990) Cell-free protein sorting to the regulated and constitutive secretory pathways. *Cell*, **60**, 837–847.
15. Jung, L.J. and Scheller, R.H. (1991) Peptide processing and targeting in the neuronal secretory pathway. *Science*, **251**, 1330–1335.
16. Regnier-Vigouroux, A., Tooze, S.A. and Huttner, W.B. (1991) Newly synthesized synaptophysin is transported to synaptic-like microvesicles via constitutive secretory vesicles and the plasma membrane. *EMBO J.*, **10**, 3589–3601.
17. Walch-Solimena, C., Takei, K., Marek, K.L., Midyett, K., Sudhof, T.C., De Camilli, P. and Jahn, R. (1993) Synaptotagmin: a membrane constituent of neuropeptide-containing large dense-core vesicles. *J. Neurosci.*, **13**, 3895–3903.
18. Okada, Y., Yamazaki, H., Sekine-Aizawa, Y. and Hirokawa, N. (1995) The neuron-specific kinesin superfamily protein KIF1A is a unique monomeric motor for anterograde axonal transport of synaptic vesicle precursors. *Cell*, **81**, 769–780.
19. Bauerfeind, R., Ohashi, M. and Huttner, W.B. (1994) Biogenesis of secretory granules and synaptic vesicles. Facts and hypothesis. *Ann. N.Y. Acad. Sci.*, **733**, 233–244.
20. Kyte, J. and Doolittle, R.F. (1982) A simple method for displaying the hydropathic character of a protein. *J. Mol. Biol.*, **157**, 105–132.
21. Stuart, A.D., Eustace, H.E., McKee, T.A. and Brown, T.D.K. (2002) A novel cell entry pathway for a DAF-using human enterovirus is dependent on lipid rafts. *J. Viol.*, **76**, 9307–9322.
22. Janes, P.W., Ley, S.C. and Magee, A.I. (1999) Aggregation of lipid rafts accompanies signaling via the T cell antigen receptor. *J. Cell Biol.*, **147**, 447–461.
23. Fortin, D.L., Troyer, M.D., Nakamura, K., Kubo, S.I., Anthony, M.D. and Edwards, R.H. (2004) Lipid rafts mediate the synaptic localization of α-synuclein. *J. Neurosci.*, **24**, 6715–6723.
24. Kenworthy, A.K., Petranova, N. and Edidin, M. (2000) High-resolution FRET microscopy of cholera toxin B-subunit and GPI-anchored proteins in cell plasma membranes. *Mol. Biol. Cell*, **11**, 1645–1655.
25. Cabrera-Poch, N., Sanchez-Ruiloba, L., Rodriguez-Martinez, M. and Iglesias, T. (2004) Lipid raft disruption triggers protein kinase C and Src-dependent protein kinase D activation and Kidins220 phosphorylation in neuronal cells. *J. Biol. Chem.*, **279**, 28592–28602.
26. Pike, L.J. and Casey, L. (1996) Localization and turnover of phosphatidylinositol 4,5-bisphosphate in caveolin-enriched membrane domains. *J. Biol. Chem.*, **271**, 26453–26456.
27. Liu, Y., Casey, L. and Pike, L.J. (1998) Compartmentalization of phosphatidylinositol 4,5-bisphosphate in low-density membrane domains in the absence of caveolin. *Biochem. Biophys. Res. Commun.*, **245**, 684–690.
28. Biskup, S., Moore, D.J., Celsi, F., Higashi, S., West, A.B., Andrabi, S.A., Kurkinen, K., Yu, S.W., Savitt, J.M., Waldvogel, H.J., *et al.* (2006) Localization of LRRK2 to membranous and vesicular structures in mammalian brain. *Ann. Neurol.*, **60**, 557–569.
29. Edidin, M. (2003) The state of lipid rafts: from model membranes to cells. *Annu. Rev. Biophys. Biomol. Struct.*, **32**, 257–283.
30. Thiele, C., Hannah, M.J., Fahrenholz, F. and Huttner, W.B. (2000) Cholesterol binds to synaptophysin and is required for biogenesis of synaptic vesicles. *Nat. Cell Biol.*, **2**, 42–49.
31. Chamberlain, L.H., Burgoyne, R.D. and Gould, G.W. (2001) SNARE proteins are highly enriched in lipid rafts in PC12 cells: implications for the spatial control of exocytosis. *Proc. Natl. Acad. Sci. USA*, **98**, 5619–5624.
32. Tooze, S.A., Martens, G.J. and Huttner, W.B. (2001) Secretory granule biogenesis: rafting to the SNARE. *Trends Cell Biol.*, **11**, 116–122.
33. Garofalo, T., Giammarioli, A.M., Misasi, R., Tinari, A., Manganelli, V., Gambardella, L., Pavan, A., Malorni, W. and Sorice, M. (2005) Lipid microdomains contribute to apoptosis-associated modifications of mitochondria in T cells. *Cell Death Differ.*, **12**, 1378–1389.
34. Simons, K. and Toomre, D. (2000) Lipid rafts and signal transduction. *Nat. Rev. Mol. Cell Biol.*, **1**, 31–39.
35. Ikonen, E. (2001) Roles of lipid rafts in membrane transport. *Curr. Opin. Cell Biol.*, **13**, 470–477.
36. Helms, J.B. and Zurzolo, C. (2004) Lipids as targeting signals: lipid rafts and intracellular trafficking. *Traffic*, **5**, 247–254.
37. Zerial, M. and McBride, H. (2001) Rab proteins as membrane organizers. *Nat. Rev. Mol. Cell Biol.*, **2**, 107–117.
38. Triantafilou, K. and Triantafilou, M. (2003) Lipid raft microdomains: key sites for Coxsackievirus A9 infectious cycle. *Virology*, **317**, 128–135.
39. Mineo, C., James, G.L., Smart, E.J. and Anderson, R.G. (1996) Localization of epidermal growth factor-stimulated Ras/Raf-1 interaction to caveolae membrane. *J. Biol. Chem.*, **271**, 11930–11935.
40. Gil, C., Soler-Jover, A., Blasi, J. and Aguilera, J. (2005) Synaptic proteins and SNARE complexes are localized in lipid rafts from rat brain synaptosomes. *Biochem. Biophys. Res. Commun.*, **329**, 117–124.
41. Salaun, C., Gould, G.W. and Chamberlain, L.H. (2005) Lipid raft association of SNARE proteins regulates exocytosis in PC12 cells. *J. Biol. Chem.*, **280**, 19449–19453.
42. MacLeod, D., Dowman, J., Hammond, R., Leete, T., Inoue, K. and Abeliovich, A. (2006) The familial Parkinsonism gene *LRRK2* regulates neurite process morphology. *Neuron*, **52**, 587–593.
43. Tsui-Pierhala, B.A., Encinas, M., Milbrandt, J. and Johnson, E.M. Jr. (2002) Lipid rafts in neuronal signaling and function. *Trends Neurosci.*, **25**, 412–417.
44. Kahle, P.J., Neumann, M., Ozmen, L., Muller, V., Jacobsen, H., Schindzielorz, A., Okochi, M., Leimer, U., van Der Putten, H., Probst, A. *et al.* (2000) Subcellular localization of wild-type and Parkinson's disease-associated mutant α-synuclein in human and transgenic mouse brain. *J. Neurosci.*, **20**, 6365–6373.
45. Kubo, S.I., Kitami, T., Noda, S., Shimura, H., Uchiyama, Y., Asakawa, S., Minoshima, S., Shimizu, N., Mizuno, Y. and Hattori, N. (2001) Parkin is associated with cellular vesicles. *J. Neurochem.*, **78**, 42–54.

46. Fallon, L., Moreau, F., Croft, B.G., Labib, N., Gu, W.J. and Fon, E.A. (2002) Parkin and CASK/LIN-2 associate via a PDZ-mediated interaction and are co-localized in lipid rafts and postsynaptic densities in brain. *J. Biol. Chem.*, **277**, 486–491.
47. Abeliovich, A., Schmitz, Y., Farinas, I., Choi-Lundberg, D., Ho, W.H., Castillo, P.E., Shinsky, N., Verdugo, J.M., Armanini, M., Ryan, A. *et al.* (2000) Mice lacking α-synuclein display functional deficits in the nigrostriatal dopamine system. *Neuron*, **25**, 239–252.
48. Itier, J.M., Ibanez, P., Mena, M.A., Abbas, N., Cohen-Salmon, C., Bohme, G.A., Laville, M., Pratt, J., Corti, O., Pradier, L. *et al.* (2003) Parkin gene inactivation alters behaviour and dopamine neurotransmission in the mouse. *Hum. Mol. Genet.*, **12**, 2277–2291.
49. Sato, S., Chiba, T., Nishiyama, S., Kakiuchi, T., Tsukada, H., Hatano, T., Fukuda, T., Yasosima, Y., Kai, N., Kobayashi, K. *et al.* (2006) Decline of striatal dopamine release in parkin-deficient mice shown by Ex Vivo autoradiography. *J. Neurosci. Res.*, **84**, 1350–1357.
50. Kubo, S.I., Nemani, V.M., Chalkley, R.J., Anthony, M.D., Hattori, N., Mizuno, Y., Edwards, R.H. and Fortin, D.L. (2005) A combinatorial code for the interaction of α-synuclein with membranes. *J. Biol. Chem.*, **280**, 31664–31672.
51. Shimura, H., Schlossmacher, M.G., Hattori, N., Frosch, M.P., Trockenbacher, A., Schneider, R., Mizuno, Y., Kosik, K.S. and Selkoe, D.J. (2001) Ubiquitination of a new form of α-synuclein by parkin from human brain: implications for Parkinson's disease. *Science*, **293**, 263–269.
52. Smith, W.W., Pei, Z., Jiang, H., Moore, D.J., Liang, Y., West, A.B., Dawson, V.L., Dawson, T.M. and Ross, C.A. (2005) Leucine-rich repeat kinase 2 (LRRK2) interacts with parkin, and mutant LRRK2 induces neuronal degeneration. *Proc. Natl. Acad. Sci. USA*, **102**, 18676–18681.
53. Valente, E.M., Abou-Sleiman, P.M., Caputo, V., Muqit, M.M., Harvey, K., Gispert, S., Ali, Z., Del Turco, D., Bentivoglio, A.R., Healy, D.G. *et al.* (2004) Hereditary early-onset Parkinson's disease caused by mutations in PINK1. *Science*, **304**, 1158–1160.
54. Hatano, Y., Li, Y., Sato, K., Asakawa, S., Yamamura, Y., Tomiyama, H., Yoshino, H., Asahina, M., Kobayashi, S., Hassin-Baer, S. *et al.* (2004) Novel PINK1 mutations in early-onset parkinsonism. *Ann. Neurol.*, **56**, 424–427.
55. Silvestri, L., Caputo, V., Bellacchio, E., Atorino, L., Dallapiccola, B., Valente, E.M. and Casari, G. (2005) Mitochondrial import and enzymatic activity of PINK1 mutants associated to recessive parkinsonism. *Hum. Mol. Genet.*, **14**, 3477–3492.
56. Hell, J.W. and Jahn, R. (1998) Preparation of synaptic vesicles from mammalian brain. Celis, J.E. (Eds), *Cell Biology*, 2nd ed. Academic Press, San Diego, Vol. 2, 102–110.

ELSEVIER

Parkinsonism and Related Disorders 14 (2008) 166–169

Parkinsonism & Related Disorders

www.elsevier.com/locate/parkreldis

Case report

Visual impairment in Parkinson's disease treated with amantadine: Case report and review of the literature

Shin-ichiro Kubo*, Akira Iwatake, Nobuyuki Ebihara, Akira Murakami, Nobutaka Hattori

Departments of Neurology and Ophthalmology, Juntendo University School of Medicine, Tokyo, Japan

Received 15 January 2007; received in revised form 17 March 2007; accepted 19 March 2007

ELSEVIER

2008

ELSEVIER

Parkinsonism and Related Disorders 14 (2008) 166–169

Parkinsonism & Related Disorders

www.elsevier.com/locate/parkreldis

Case report

Visual impairment in Parkinson's disease treated with amantadine: Case report and review of the literature

Shin-ichiro Kubo*, Akira Iwatake, Nobuyuki Ebihara, Akira Murakami, Nobutaka Hattori

Departments of Neurology and Ophthalmology, Juntendo University School of Medicine, Tokyo, Japan

Received 15 January 2007; received in revised form 17 March 2007; accepted 19 March 2007

Abstract

A 61-year-old man with Parkinson's disease (PD) developed sudden-onset visual impairment after initiation of amantadine treatment. Ophthalmologic examination revealed corneal endothelial edema. Discontinuation of amantadine resulted in rapid improvement of visual acuity. A review of the literature indicated only a few reports of amantadine-associated corneal dysfunction in patients with neurological disorders as well as influenza syndrome, but none with PD. Amantadine-associated visual impairment in PD could be possibly overlooked, since PD mainly affects elderly people who often develop aging-related ocular changes. The present report alerts neurologists and physicians in general to the peculiar ophthalmologic side effect of amantadine.

Keywords: Amantadine; Corneal endothelial dysfunction; Side effects; Parkinson's disease

1. Introduction

Parkinson's disease (PD) is the second most common neurodegenerative disease after Alzheimer's disease, affecting ~0.3% of the general population and 3% of people over the age of 65 [1]. The disease is characterized pathologically by loss of dopaminergic neurons in the substantia nigra pars compacta in the midbrain and phenomenologically by parkinsonism such as resting tremor, muscular rigidity, bradykinesia, and postural instability. Amantadine, an antagonist of *N*-methyl-D-aspartate (NMDA)–glutamate receptor [2], is widely used for the treatment of PD including levodopa-induced dyskinesias [3], since its anti-parkinsonian effects were reported in 1969 [4]. However, there have been few reports in the literature of ocular side effects of amantadine. We describe a rare case of a patient with PD who developed visual disturbance during treatment with amantadine.

2. Case report

A 61-year-old man presented with gradual left-sided shuffling gait. Twenty-five months after the onset, the patient noticed a mild resting tremor in the left hand and complained of a tendency for the left leg to stumble. He consulted a local neurologist 30 months after symptom onset and was diagnosed with PD. The patient was then started on treatment with amantadine (300 mg/day) and trihexyphenidyl (4 mg/day). At age 64, he was referred to the outpatient clinic of our hospital for a second opinion.

At that time, systemic examination was normal but neurological examination showed facial hypomimia, pill-rolling resting tremor of the left hand, and left-side bradykinesia. The patient dragged the left leg on walking with a slightly diminished left arm swing. He showed stooped posture, but postural reflex was preserved. He was alert and oriented, but was slightly slow to respond to questions. There were no cerebellar signs, the deep tendon reflexes were intact in all extremities, and the plantar responses were flexor. Sensory function was intact. The patient complained of constipation and impaired olfaction. Routine hematological and biochemical tests were normal. Magnetic resonance imaging of the brain showed no abnormality. Cardiac uptake of ^{123}I-metaiodobenzylguanidine was reduced. Based on these findings, the patient was diagnosed as having PD.

Eight months after commencement of amantadine treatment, the patient noticed sudden deterioration in

*Corresponding author. Tel.: +81 3 3813 3111; fax: +81 3 5684 0476.
E-mail address: skubo@med.juntendo.ac.jp (S.-i. Kubo).

1353-8020/$ - see front matter © 2007 Elsevier Ltd. All rights reserved.
doi:10.1016/j.parkreldis.2007.03.003

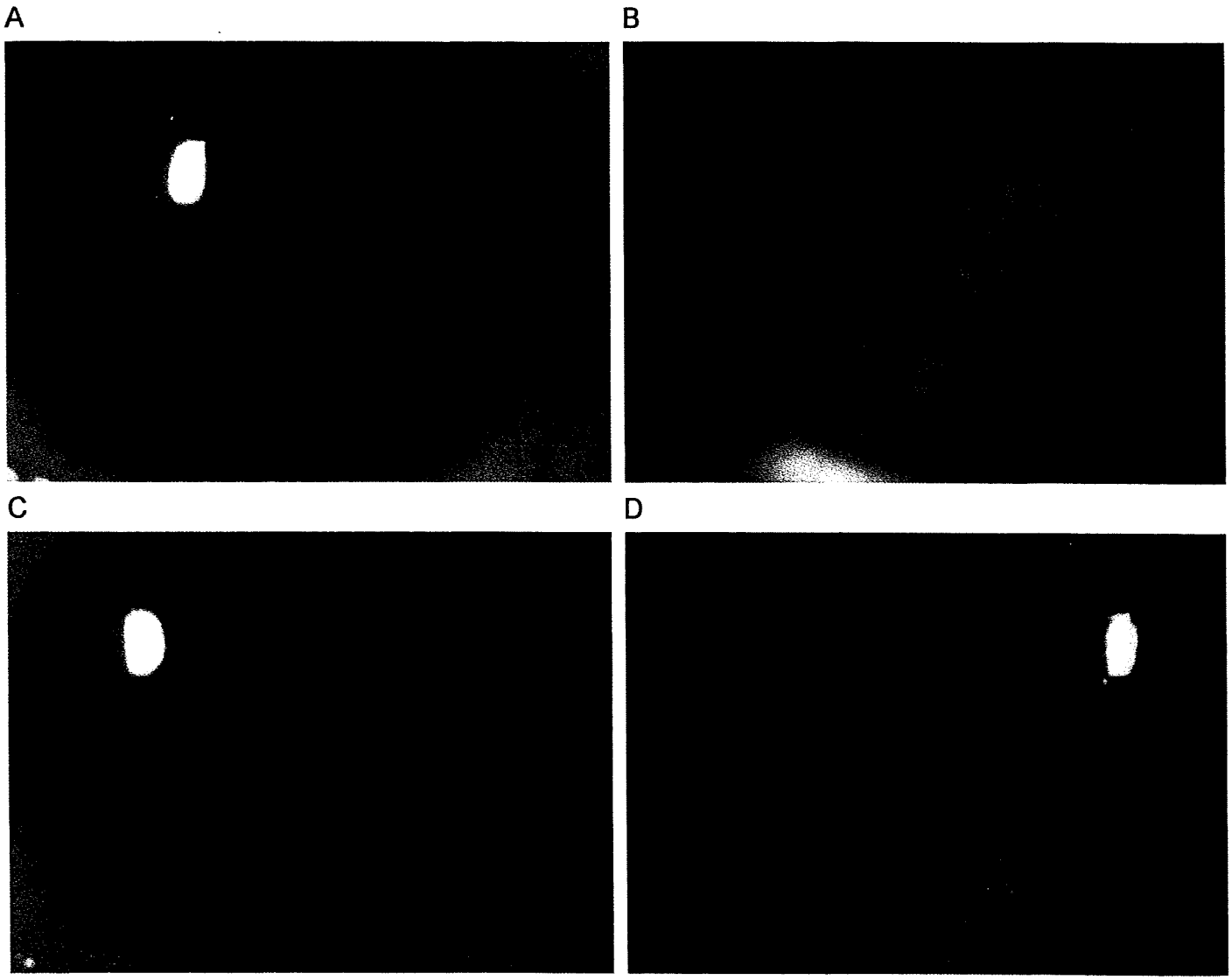

Fig. 1. Ophthalmologic examination conducted upon the complaint of sudden deterioration of visual acuity: (A) right cornea, (B) right cornea (slit-lamp examination). Note the presence of corneal edema and endothelial damage, (C) left cornea, and (D) left cornea (slit-lamp examination). Note corneal edema and endothelial damage.

visual acuity reflected by inability to read the small print of newspapers. He was referred urgently to the ophthalmology department at our hospital. Ophthalmologic examination revealed bilateral corneal endothelial damage and edema (Fig. 1A–D). Visual acuity for the left and right eye was 0.2 (OD) and 0.1 (OS), respectively. There were no signs of inflammation such as conjunctival redness, cells, or flare in the anterior chambers. Occlusion of the iridocorneal angles was ruled out, although the patient was taking trihexyphenidyl, an anti-cholinergic drug. The ophthalmologist indicated possible ocular side effect associated with amantadine. Accordingly, amantadine was tapered off in 3 days. Corneal endothelial damage and edema began to improve gradually and returned to normal with visual acuity of 1.0 (OD) and (1.2) (OS) at 8 days after discontinuation of amantadine (Fig. 2A–D), although resting tremor in the left hand slightly worsened.

3. Discussion

Amantadine, which was developed as a drug for influenza A virus in 1959, was later incidentally found to exhibit anti-parkinsonian effect in 1968 [4]. Since then, amantadine has been used in the management of PD worldwide. Notably, amantadine in addition to sulpiride [5] is pharmacologic therapy available for levodopa-induced dyskinesias, one of the motor complications in advanced stages of the disease [6]. Despite its frequent usage, there are only a few case reports of amantadine-associated visual impairment [7–11]. In these reported cases, the diseases associated with the development of amantadine-related visual impairment included essential tremor [7], influenza syndrome [8], vascular parkinsonism [10], and unknown neurological disorder presenting with tremor [11]. Surprisingly, there is no reported case with PD.

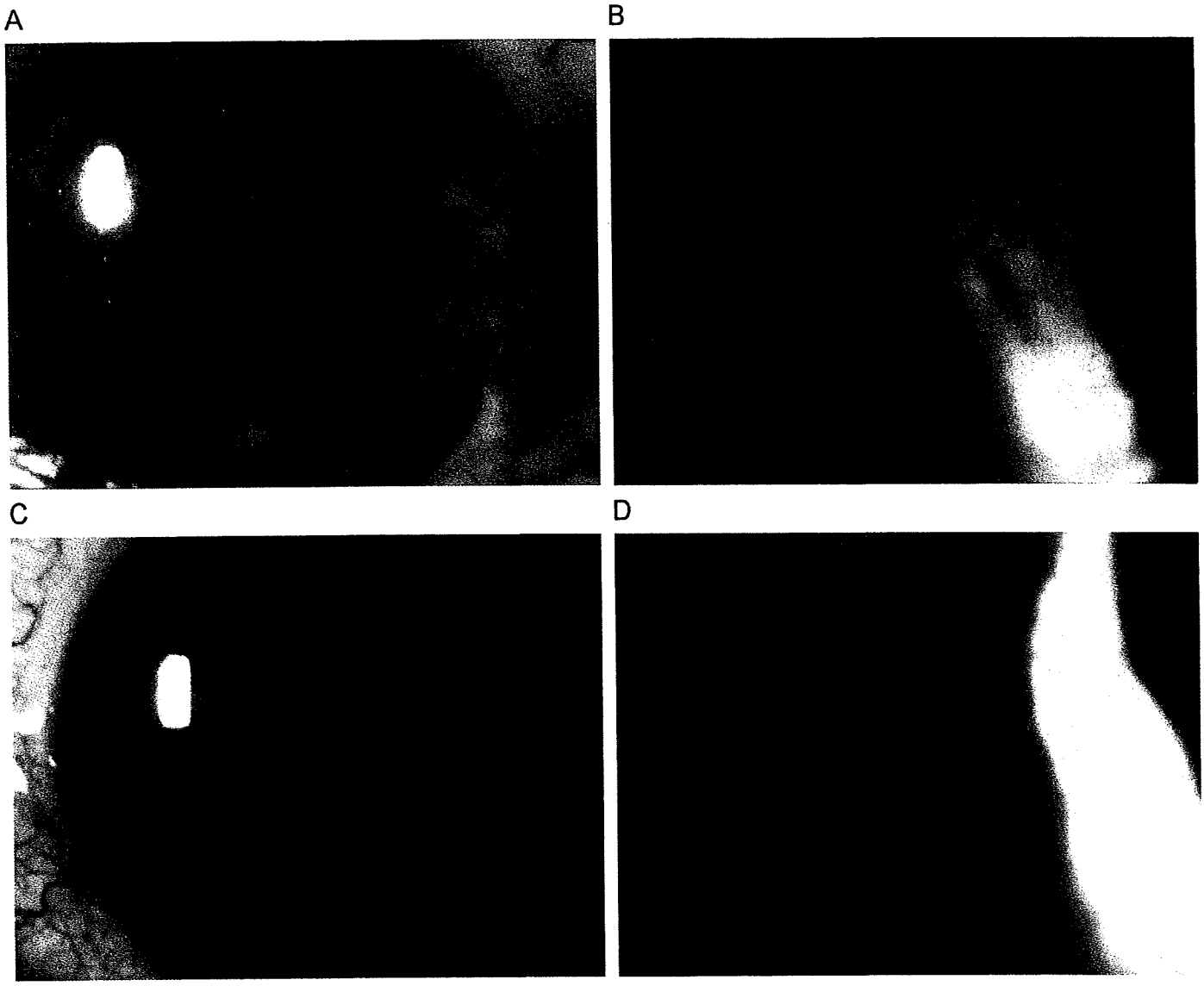

Fig. 2. Ophthalmologic examination conducted 8 days after discontinuation of amantadine: (A) right cornea, (B) right cornea (slit-lamp examination). Compare with Fig. 1 and note the disappearance of abnormal finding in the cornea, (C) left cornea, and (D) left cornea (slit-lamp examination). No abnormal finding is found in the cornea.

To our knowledge, our patient is the first reported PD case with visual impairment associated with amantadine. Based on the evidence that PD mainly affects elderly people, it is possible that PD patients with amantadine-associated visual impairment are misdiagnosed as aging-related ocular changes such as presbyopia and cataract.

Although the mechanism of amantadine-induced impaired vision remains poorly understood, there is no doubt in our case and in the reported cases about the relationship between amantadine and corneal dysfunction. In all cases, visual acuity recovered within a few weeks on cessation of the drug and such clinical improvement was associated with improvement in corneal lesions such as corneal endothelial or epithelial edema and superficial punctate keratitis [7–11]. Furthermore, resumption of amantadine was reported to result in recurrence of visual impairment [9,10], emphasizing such relationship. In previous reports, the dosage of amantadine was 100–400 mg/day comparable with that in our patient, and the interval between commencement of amantadine and appearance of visual symptoms was 1–3 weeks [7–11]. However, in the present case, the visual impairment developed 8 months after initiation of amantadine, suggesting that careful follow-up including ophthalmologic assessment is required whenever patients are under treatment of the drug. It is noteworthy that amantadine-associated visual impairment was of sudden onset and that amantadine did not cause permanent damage since such impairment disappeared within a few weeks after discontinuation of the drug therapy in our patient as well as reported cases.

In conclusion, amantadine can cause impairment of corneal endothelial function and needs to be considered in the differential diagnosis of visual impairment. As age is an important risk factor in PD, with the increasing age of the